Dislocations and morphological instabilities: Continuum modeling of misfitting heteroepitaxial films

Mikko Haataja,[1,*] Judith Müller,[2] A. D. Rutenberg,[3] and Martin Grant[1]
[1]*Centre for the Physics of Materials, Department of Physics, McGill University, Rutherford Building, 3600 rue University, Montréal, Québec H3A 2T8, Canada*
[2]*Instituut-Lorentz for Theoretical Physics, University of Leiden, P.O. Box 9506, NL-2300 RA, Leiden, The Netherlands*
[3]*Department of Physics, Dalhousie University, Halifax, Nova Scotia B3H 3J5, Canada*
(Received 5 November 2001; published 5 April 2002)

We present a continuum model of nonequilibrium heterogeneous elastic systems, which includes both smooth and singular strains, as well as their coupling to free surfaces, in two spatial dimensions. It accurately includes nucleation, interactions, and dynamics of dislocations. In particular, we demonstrate that the model recovers the well-known Matthews-Blakeslee critical thickness for the nucleation of misfit dislocations. For misfitting heteroepitaxial films above the critical thickness, dislocations compete with the stress-induced instability of the film-vapor interface as a strain-relief mechanism. At early times, the dislocations slow down the initial instability by climbing to the film-substrate interface and relaxing the misfit strain partially. However, the late-time morphology is determined by the strong interaction between the stress concentration at the bottom of the grooves and the singular stresses due to dislocations.

DOI: 10.1103/PhysRevB.65.165414 PACS number(s): 62.20.Fe, 64.60.My, 68.55.−a

I. INTRODUCTION

The precise control of the morphology of thin films under strain is an important ingredient in the fabrication of microelectronics. For example, various semiconductor alloys are commonly used to engineer devices with particular values of the band gap. Due to the misfit in the constituent's lattice constants and silicon, the most commonly used substrate, the film is typically under a compressive misfit stress. It is now understood that such strained films may undergo a morphological instability owing to the stress in the film. This instability, known as the Asaro-Tiller-Grinfeld[1,2] (ATG) instability, allows the film to partially relax its elastic energy by becoming corrugated (''buckling''), thereby making the growth of planar films difficult to achieve.[3–9] An alternative strain-relief mode can be important for a sufficiently thick film:[10–13] misfit dislocations can nucleate and climb to the film-substrate interface, thereby relaxing strain. This latter mechanism leads typically to a large number of threading dislocations that can deteriorate the electrical properties of the film.

For some applications, films need not be grown planar. For example, there is a growing need to manufacture small-scale quantum dots ($L \sim 1-10$ nm), which can be used in such novel optoelectronic devices as single-electron transistors, quantum-well lasers, and light-emitting diodes. These nanoscale components have been traditionally obtained from planar films by lithographic techniques. However, such lithographic techniques incur practical limitations as the size of the desired device is decreased. Hence it has been suggested that one can employ the ATG instability as a means to self-assemble regular patterns. In that case, the size and spatial arrangement of the islands determines the optoelectronic properties of the device. Therefore, there is a need for a better understanding of how the growth conditions and materials parameters affect the final morphology of the film.

Experiments suggest[9,14–17] that both of these mechanisms—the buckling of the film and the nucleation of dislocations—take place in supercritical films. It has been demonstrated[17] recently that groove alignment in $Si_{1-x}Ge_x$ films grown on a Si surface depends crucially upon whether misfit dislocations are present or not. In particular, the dislocations line up at the film-substrate interface in the $\langle 110 \rangle$ direction, and modify the overall strain pattern in such a way that the subsequent growth of the film occurs on top of the dislocations. Even a qualitative understanding of the morphology requires an approach that treats explicitly both mechanisms at the same time.

To this end, in this paper we introduce a continuum model that treats both strain-relief mechanisms on an equal footing. It implicitly includes the nonlinearities arising from free surfaces, as well as singular interactions between dislocations and smooth misfit strains. The interaction between nonuniform stresses and plasticity is theoretically challenging to address, since the former constitutes a free-boundary problem, while the latter involves singular contributions to the strain. In order to overcome the first difficulty, we have employed a continuum model based on the order-parameter (or phase-field) concept that implicitly takes free boundaries into account. In order to overcome the second difficulty, we introduce a ghost field that conveniently mediates the singular interaction between the dislocations. We give the model a detailed exposition, as well as report on some numerical tests with the model. In particular, it is numerically demonstrated that our model recovers the well-known Matthews-Blakeslee criterion for the nucleation of misfit dislocations. Furthermore, it is shown that the model accurately incorporates dislocation interactions in thin films.

After reporting results pertaining to dislocation energetics in a static film, we apply the model to the dynamics of thin-film growth in the presence of dislocations. We show that, depending on their mobility and density, dislocations can have a strong effect on the dynamics. In particular, we dem-

onstrate that the film-vapor interface may be stabilized due to the presence of misfit dislocations, if the dislocations screen the misfit stress completely. The effect of dislocations can be tuned by varying the mobility, or the density of dislocations, through their core energy. We find that dislocations generally coexist with the ATG instability. The growth rates of the instability can be continuously tuned by dislocation mobility and core energy. In the nonlinear regime, defects lead to slower coarsening of the morphology due to a buildup of dislocations ahead of the groove tips.

This paper is organized as follows. First, in Sec. II we discuss the two modes of strain relief in thin-film growth, and the concepts of critical thickness and the ATG instability. In Sec. III we review related work. The model is given a detailed exposition in Sec. IV. Our results are summarized in Sec. V, for both static and evolving films. It is shown numerically that the Matthews-Blakeslee condition is recovered for dislocations in a static planar film. Furthermore, the coupled dynamics of the thin film and dislocations are studied numerically. The paper ends with a conclusion and discussion in Sec. VI. Mathematical details are given in the Appendices.

II. STRAIN-RELIEF MECHANISMS

A. Misfit dislocations and the critical thickness

If a film is grown on a substrate with a different lattice constant, that epilayer will usually be strained. It is well known that, for thick enough films, threading dislocations extend to the film-substrate interface and relax the misfit stress in the film by destroying the coherency of the film-substrate interface.[10–12,18] Below this thickness, dislocations are thermodynamically unstable and the system must revert to some other means to relax the stress.

Partially relaxing coherency at the interface allows the lattice constant in the epilayer to approach its equilibrium value. However, locations where coherency is lost correspond to dislocations. Hence, misfit strain is partially screened by the interfacial misfit dislocations. This leads to an overall decrease in the net misfit strain and hence strain energy. Upon employing energy-balance arguments, Matthews and Blakeslee[12,13] derived the following expressions for the critical thickness h_c and the residual equilibrium strain f^*:

$$h_c = \frac{\mu b}{4\pi \mathcal{Y} f} \ln(h_c/b) + \text{const} \tag{1}$$

and

$$f^* = \frac{\mu b}{4\pi \mathcal{Y} h} [\ln(h/b) + 1]. \tag{2}$$

Note that, in general, $f^* \neq 0$, which implies that the strain is only partially relaxed by the dislocations. Typically, $h_c \sim 10$ atomic layers for a misfit strain $f \approx 0.1$. Dynamically, defects are expected to nucleate at the film-vapor interface and glide down to the film-substrate interface. Experiments of Gao and Nix[9] demonstrated that films can be grown past their nominal critical thicknesses due to kinetic limitations on dislocation formation. However, upon annealing, they observed dislocation nucleation, in addition to a morphological instability of the initially flat surface. This will be discussed further below.

B. Asaro-Tiller-Grinfeld instability of coherent subcritical films

While misfit dislocations are expected to relax the misfit strain partially for films of thickness $h > h_c$, the system can also relax its total energy through a morphological ATG instability.[1–3,7] This mode occurs in films below their critical thickness. As a consequence of this instability, the free interface develops grooves and islands form with a well-defined wavelength, while the film-substrate interface remains coherent. This mode has been identified[19] with dislocation-free layer and island (Stranski-Krastanov) growth.

Consider a semi-infinite two-dimensional film,[1–3,20,21] where the interface is given by $y = h(x)$ in the $\vec{r} = (x,y)$ plane and $h(x) = h_0 \sin(qx)$ where q is a wave number. The boundary conditions on the stress are $\sigma_{xx}(x, y \to -\infty) = \sigma_{\text{ext}}$ and $\sigma_{yy}(x, y \to -\infty) = \sigma_{xy}(x, y \to -\infty) = 0$, which gives rise to a uniaxial stress in the unperturbed film. Furthermore, assume that the interface is traction-free, i.e., $\sigma_{ij} n_j = 0$, or $\sigma_{nn} = \sigma_{nt} = 0$, where $\hat{n}$ denotes the unit normal to the interface, $\hat{t}$ denotes the tangential direction, and a summation convention is implicit over repeated indices. The resulting tangential stress at the interface is $\sigma_{tt} = \sigma_{ext}[1 - 2qh_0 \sin(qx)] + O(h_0^2 q^2)$. In particular, this equation implies that the perturbation of the free interface leads to a stress concentration at the valleys, while the stress is relaxed at the hilltops. This stress gradient can drive mass flux from the valleys to the hills, hence increasing corrugation. At sufficiently short-length scales, the surface tension γ suppresses the instability. The typical scale λ of the grooved pattern can be obtained by carrying out a linear-stability analysis. A straightforward calculation[21] yields $\sim \gamma \mathcal{Y} / \sigma_{\text{ext}}^2$. For a typical misfit strain of $f = 0.1$, this implies $\lambda \sim 100$–1000 Å.

Ozkan *et al.*[17] have clearly illustrated the importance of interactions between the smooth strains and dislocations. In particular, in the case of supercritical films, initially the film roughens as subcritical ones. However, the grooves act as preferred nucleation sites for misfit dislocations,[9,14–16] and once these dislocations are located at the film-substrate interface, they modify the strain distribution in the film that eventually causes the surface ridges to align with the dislocations. Therefore, in order to understand the evolution of the morphology it is important to consider both mechanisms on an equal footing.

III. REVIEW OF RELATED WORK

Since the discovery of the ATG instability and the role of misfit dislocations in strain relief, they have been studied and discussed by various authors.[9] Spencer *et al.*[4] performed a linear-stability analysis of a growing epitaxially strained dislocation-free solid film, and determined the conditions for which a growing film is unstable. Guyer and Voorhees[6] studied a model of alloy thin film growing by deposition flux from the vapor, and also carried out a linear-stability analysis for the free surface. They demonstrated that, contrary to

single-component films, under certain conditions, tensile misfit strain can completely stabilize a growing film, whereas compressive strains of the same magnitude would be destabilizing.

To address nonlinearities, Yang and Srolovitz[5,22] derived an evolution equation for the free surface of a two-dimensional system and found numerically that deep, cracklike grooves form as a result of the instability. In particular, they observed accelerating grooves with finite-time singularities manifested in the apparent divergence of the groove growth rate. However, they did not study the evolution of the interface in the grooved regime. To this end, two of us[7] proposed a model, free from numerical instabilities, based on the Ginsburg-Landau approach to study the strain-relief mechanism at a free surface in two and three dimensions. The model permitted the simulation of the surface instability, and the subsequent competitive coarsening of the interface in the nonlinear regime, in qualitative agreement with experiments of Gao and Nix.[9] Furthermore, this technique made three-dimensional simulations possible. A model similar in spirit was proposed and studied by Kassner and co-workers.[8,23]

The role of misfit dislocations in the strain-relief mechanism of thin films was addressed by Dong *et al.*,[24] who studied the growth and relaxation of two-dimensional misfitting films through molecular-dynamics simulations. They demonstrated that, above a critical thickness, dislocations nucleate and relax most of the misfit. They also demonstrated that the surface morphology plays an important role in the nucleation of dislocations, in which the formation of deep-valley structures acted as preferential nucleation sites for dislocations. However, due to small (microscopic) length and time scales amenable to molecular-dynamics simulations, they did not address the physics in the nonlinear regime where both coarsening and misfit dislocations and their interactions contribute to the morphology of the film.

A different type of approach to studying dynamics of dislocations in three dimensions under external stresses was undertaken by Schwarz,[25] where the motion of dislocation lines is driven by the net local stress through the Peach-Koehler force. While treating the interactions and topology of the dislocation network physically, the motion of the dislocations was not coupled to the evolution of a free surface, and therefore, the response of the free surface to both nonsingular and singular stresses could not be addressed.

All of the approaches presented above have some inherent shortcomings. Continuum models presented to date[4–8] only include smooth elastic fields, and dislocations have been omitted. The molecular-dynamics simulations of Dong *et al.*[24] include dislocations implicitly. However, length and time scales amenable to molecular-dynamics studies are quite short ($\sim 10^{-7}$ m and $\sim 10^{-8}$ s). Therefore, it is worthwhile to develop a coarse-grained continuum formulation, free from length and time-scale restrictions, which is able to treat smooth elastic strains as well as the nucleation, interaction, and dynamics of dislocations in heterogeneous strained systems. As discussed above, this approach necessarily leads to a free-boundary problem with singular long-ranged elastic fields. A continuum approach constitutes a minimal model whose generic features are applicable to many microscopically different systems.[26]

IV. MODEL

Our approach is based on the phase-field method employed by two of us[7] and Kassner and co-workers[8,23] to model the ATG instability, in the absence of dislocations. A preliminary account of some aspects of this work can be found in Ref. 27. We couple a scalar vapor-solid order parameter to vectorial displacement and dislocation density fields, including an elastically inert solid substrate. Dislocations are characterized by a vector field $\vec{b}(\vec{r})$, which gives the local Burger's vector density. Dislocations give rise to and interact through singular stresses; in particular, upon assuming mechanical equilibrium, one can relate $\vec{b}(\vec{r})$ to the singular part of the stress tensor through the Airy stress function.[28] Moreover, correct and accurate treatment of these singular interactions is essential. To this end, we make use of and generalize the continuum model introduced by Aguenaou[29] to study dislocations and their interactions in two spatial dimensions. In particular, we introduce an auxiliary field that mediates the nonlocal interaction between the dislocations. This field is massive (and hence short ranged) in the vapor phase, while becoming massless (long ranged) in the solid phases. As shown below, this is sufficient to make the dislocation interactions vanish in the vapor phase, as required. It leads to the correct logarithmic dependence of the dislocation self-energy on the thickness of the film, which is essential in order to recover the Matthews-Blakeskee critical thickness. Furthermore, in our approach, dislocations are coupled to the external stresses via standard elastic interaction; this provides a thermodynamic driving force for the nucleation of dislocations.

Dynamic fields included explicitly in the model are a scalar solid-vapor order parameter ϕ, the Burger's vector field $\vec{b}(\vec{r})$ for the dislocations, and six components for the nonsingular and singular stresses. Upon employing mechanical equilibrium conditions, however, the only explicitly time-dependent fields are ϕ and $\vec{b}$; smooth strains are expressed in terms of ϕ. Singular stresses and their interaction with nonsingular strains are determined through ϕ and $\vec{b}$ by introducing two auxiliary fields that are equilibrated instantaneously or equivalently, on a time scale much shorter than typical time scales corresponding to the evolution of the surface. Physically, this corresponds to the assumption that the relevant dynamics is slow compared to the speed of sound; this condition is most certainly valid in typical experiments where the evolution of the surface occurs over several minutes or hours.[9,17]

An important feature of the model is that, since dislocations are topological defects, their dynamics must satisfy a conservation law for the total Burger's vector, leading to diffusive dynamics. This allows us to study the effect of defect mobility on the pattern forming system. Furthermore, we assume that evaporation condensation is the main mechanism for mass transport to and from the film, leading to nonconserved dynamics for the solid-vapor order parameter.

This interplay between conserved dislocations and nonconserved mass leads to interesting effects, such as mobility-dependent ductility: in Ref. 27 it is shown that, depending on their mobility, defects can screen stress by building up at large-curvature groove tips, leading to high ductility, or be ''outrun'' by the tips, leading to brittleness via a nonequilibrium brittle-to-ductile transition. Finally, we consider an external deposition flux that allows us to study both annealed systems and systems with deposition.

A. Statics

As a generic model for the energetics of strained thin films, the free-energy functional is constructed such that it describes a strained solid-vapor system with coexisting phases, and dislocations interacting with each other, and with the nonsingular strains in a finite film. We write $\mathcal{F}$ as the sum of seven terms:[21,28–30]

$$\mathcal{F}=\mathcal{F}_{\phi}+\mathcal{F}_{\rm ext}+\mathcal{F}_{\rm el}+\mathcal{F}_{\rm int}+\mathcal{F}_{\rm loc}+\mathcal{F}_{\rm coup}+\mathcal{F}_{\rm flux}. \tag{3}$$

Phase coexistence of solid, film, and vapor is described by the term involving the order parameter ϕ,

$$\mathcal{F}_{\phi}=\int d\vec{r}\left[\frac{\epsilon^2}{2}|\vec{\nabla}\phi|^2+f(\phi)+\frac{\eta_0^2}{2\kappa}\Phi_{\rm mis}^2\right], \tag{4}$$

where $f(\phi)=(1/a)\phi^4(\phi-1)^2(\phi-2)^2$, a is a constant, κ is the compressibility modulus, and η_0 is proportional to the externally applied stress. Hence, the homogeneous equilibrium phases of the vapor, film, and solid substrate correspond to $\phi_{\rm eq}=0$, 1, or 2, respectively. For an inhomogeneous system, these coexisting phases will be separated by diffuse interfaces of thickness $w\sim\epsilon\sqrt{a}$. The phase-field approach is equivalent to the sharp-interface formulation as long as the interface thickness is much smaller than typical length scales of interest in the morphology.[31] We introduce $\Phi_{\rm mis}$ and $\Phi_{\rm sol}$ to enforce convenient thermodynamics for the vapor, film, and solid substrate equilibrium phases, generalizing the approach of Kobayashi.[32] The quantity $\Phi_{\rm mis}$ ensures that the stress only occurs at a misfit; $\Phi_{\rm sol}$ ensures that only the two solid phases can support shear. This is done by requiring $\Phi'(\phi_{\rm eq})=0$, where the prime denotes a derivative, and $\Phi(\phi_{\rm eq})=\phi_{\rm eq}$, for $\phi_{\rm eq}=0$ or 1, while for $\phi_{\rm eq}=2$, $\Phi_{\rm mis}=0$ and $\Phi_{\rm sol}=1$. These requirements are satisfied by the choices

$$\Phi_{\rm mis}=-\tfrac{1}{11}(2\phi^6-12\phi^5+15\phi^4+20\phi^3-36\phi^2), \tag{5}$$

and

$$\Phi_{\rm sol}=-\tfrac{3}{132}(19\phi^6-81\phi^5+60\phi^4+135\phi^3-177\phi^2). \tag{6}$$

The externally applied stress enters through

$$\mathcal{F}_{\rm ext}=\int d\vec{r}[\,\eta_0\Phi_{\rm mis}\vec{\nabla}\cdot\vec{u}^{ns}]. \tag{7}$$

This ''prestress'' leads to nonzero stresses in the epilayer; the strength of the applied stress is determined by the coupling constant η_0. We assume that all of the misfit strain is accommodated by the film. This assumption is justified as long as the film thickness is much less than the thickness of the substrate layer. Smooth nonsingular elastic fields are described by

$$\mathcal{F}_{\rm el}=\int d\vec{r}\left[\frac{1}{2}\kappa(\vec{\nabla}\cdot\vec{u}^{ns})^2+\mu\Phi_{\rm sol}\left(u_{ij}^{ns}-\frac{\delta_{ij}}{2}\vec{\nabla}\cdot\vec{u}^{ns}\right)^2\right], \tag{8}$$

where μ is the shear modulus.

The singular part of the elastic energy involves several terms. Interactions between dislocations are mediated by a complex auxiliary field ξ through

$$\mathcal{F}_{\rm int}=\int d\vec{r}\left[\frac{1}{2\mathcal{Y}}\xi\nabla^4\xi+\imath\xi\eta+\frac{1}{2\mathcal{Y}l^4}(1-\Phi_{\rm sol})\xi^2\right], \tag{9}$$

where $\mathcal{Y}$ is the Young's modulus and l is a microscopic length entering into the boundary conditions for ξ at the free surfaces, as shown in Appendix E. Below we relate ξ to the Airy stress function. Once integrated out,[29] this gives rise to the nonlocal interaction between the dislocations, as demonstrated below. Back coupling of the defects to the stress involves the field

$$\eta(\vec{r})=\Phi_{\rm sol}(\nabla_x b_y-\nabla_y b_x). \tag{10}$$

The local energy of a dislocation enters through

$$\mathcal{F}_{\rm loc}=\int d\vec{r}[\,c\vec{b}^2(\vec{b}^2-b_0^2)^2+E_c\vec{b}^2], \tag{11}$$

where b_0 is the size of the dislocation, which is set by the anharmonic term, $E_c\sim b^2$ is the defectcore energy, and c is a constant that determines the barrier for the nucleation of defects. Finally, the coupling between singular strain u_{ij}^s and smooth stress σ_{ij}^{ns} is accomplished by

$$\mathcal{F}_{\rm coup}=\int d\vec{r}\,\sigma_{ij}^{ns}u_{ij}^s. \tag{12}$$

The last term in the free-energy functional describes external flux

$$\mathcal{F}_{\rm flux}=-H\int d\vec{r}\,\Phi_{\rm flux}\theta[y-h(x)], \tag{13}$$

where H is a constant, $\Phi_{\rm flux}=\frac{1}{2}\phi^2-\frac{1}{4}\phi^4$, $h(x)$ denotes the position of the stationary film-substrate interface, and θ is the Heaviside step function. This controls the flux of particles to the epilayer, permitting the study of both annealed films and films with deposition.

Nonlocal couplings between the dislocations, as expressed by the Peach-Koehler force, enter through $\mathcal{F}_{\rm int}$. This term arises from the elastic energy stored in the singular stresses, and it is merely an alternative way of writing $\mathcal{F}_{\rm int}=\frac{1}{2}\int d\vec{r}\,\sigma_{ij}^s u_{ij}^s$. This can be seen as follows. First, we note that employing the definition of the Airy stress function χ, it can be shown[33] that this is equivalent to

$$\mathcal{F}_{\rm int}=\frac{1}{2\mathcal{Y}}\int d\vec{r}(\nabla^2\chi)^2. \tag{14}$$

Since $\nabla^4\chi=\mathcal{Y}(\nabla_x b_y-\nabla_y b_x)$ for a homogeneous system,[29,33,34] it is straightforward to show that Eq. (14) can be rewritten as

$$\mathcal{F}_{\rm int}=\frac{\mathcal{Y}}{2}\int\frac{d\vec{q}}{(2\pi)^2}\frac{1}{q^2}\left(\delta_{ij}-\frac{q_iq_j}{q^2}\right)b_i(\vec{q})b_j(-\vec{q}). \quad (15)$$

Now, if ξ equilibrates instantaneously, it follows that ξ satisfies (letting $\xi\equiv{\rm Im}\,\xi$)

$$\frac{1}{\mathcal{Y}}\nabla^4\xi+\eta+\frac{1}{\mathcal{Y}l^4}(1-\Phi_{\rm sol})\xi=0. \quad (16)$$

By identifying $\chi=-\xi$, χ satisfies

$$\nabla^4\chi+\frac{1}{l^4}(1-\Phi_{\rm sol})\chi=\mathcal{Y}\eta. \quad (17)$$

For a homogeneous system, $\Phi_{\rm sol}=1$, and Eq. (16) reduces to

$$\frac{1}{\mathcal{Y}}\nabla^4\xi+\eta=0. \quad (18)$$

Equation (18) is easily solved in Fourier space, and when ξ is replaced by its solution, it can be shown,[29] that $\mathcal{F}_{\rm int}$ leads to the well-known nonlocal interaction between the dislocations, as embodied in Eq. (15).

Consider a heterogeneous system, as described by Eq. (16). Since η vanishes in the vapor phase, dislocations in that phase do not contribute to the overall stress state of the system, and hence they do not interact amongst themselves or with other dislocations in the solid phases. In addition, singular stresses due to defects in the film must vanish in the vapor phase. This is enforced conveniently by the inhomogeneous mass term in Eq. (16). In the vapor phase, we have $\nabla^4\xi+\xi/l^4=0$. In Appendix E we show that this implies exponentially decaying solutions for the dislocations in the vapor phase. Consequently, this enforces effective boundary conditions for ξ at the solid-vapor interface. In particular, we use an asymptotic expansion to show that ξ satisfies the following partial differential equation in the sharp-interface limit: $\nabla^4\xi+\mathcal{Y}\eta=0$ in the domain $\Omega=\{\phi(\vec{r})\geqslant 1\}$ with $\xi=\vec{\nabla}\xi\cdot\vec{n}=0$ in the domain $\{\phi(\vec{r})=1/2\}$.

The origin of the elastic coupling terms is straightforward. The total strain $u_{ij}^{\rm tot}$ of the system is[35] the sum of smooth (nonsingular) and singular strains, i.e., $u_{ij}^{\rm tot}=u_{ij}^{ns}+u_{ij}^{s}$. Also, the total stress can be decomposed to the sum of smooth and singular stresses: $\sigma_{ij}^{\rm tot}=\sigma_{ij}^{ns}+\sigma_{ij}^{s}$. From the theory of elasticity, it follows that the elastic energy is $\frac{1}{2}\int d\vec{r}\,\sigma_{ij}^{\rm tot}u_{ij}^{\rm tot}$, where summation over repeated indices is implied. By using the definition of $\sigma_{ij}^{\rm tot}$ and $u_{ij}^{\rm tot}$, this free energy can be rewritten as $\frac{1}{2}\int d\vec{r}\,\sigma_{ij}^{ns}u_{ij}^{ns}+\frac{1}{2}\int d\vec{r}\,\sigma_{ij}^{s}u_{ij}^{s}+\int d\vec{r}\,\sigma_{ij}^{s}u_{ij}^{ns}$. Therefore, the energy breaks up naturally into three contributions: smooth strain energy ($\mathcal{F}_{\rm el}$), singular strain energy ($\mathcal{F}_{\rm int}$), and their coupling ($\mathcal{F}_{\rm coup}$). The elastic energy of the singular strains can be written in terms of dislocation self-energies and the interactions between the dislocations, as employed by Nelson and Halperin[33,34] in their study of dislocation mediated melting in two dimensions.

B. Dynamics

We assume that the dynamics of the system is driven by the minimization of the free energy, thereby leading to relaxational dynamics for ϕ and $\vec{b}$. Mechanical equilibrium allows us to integrate out the strains; consequently, two auxiliary fields are naturally introduced. As discussed above, the interaction between the dislocations is mediated by the field ξ, and the interaction between the dislocations and smooth stresses is mediated by a new field β. These fields satisfy (see Appendix B for a derivation)

$$\nabla^4\xi+\frac{1}{l^4}(1-\Phi_{\rm sol})\xi=-\mathcal{Y}\eta,$$

$$\nabla^4\beta(\vec{r})+\frac{1}{l^4}[1-\Phi_{\rm sol}(\vec{r})]\beta(\vec{r})=\left[\frac{\delta_{ij}}{4\kappa}\nabla^2\sigma_{ij}^{ns}(\vec{r})+\left[\varepsilon_{ik}\varepsilon_{jl}\nabla_k\nabla_l\sigma_{ij}^{ns}(\vec{r})-\frac{\delta_{ij}}{2}\nabla^2\sigma_{ij}^{ns}(\vec{r})\right]\Big/2\mu\right]. \quad (19)$$

These fields are equilibrated instantaneously using an iterative scheme. Following Onuki and Nishimori,[39] Sagui *et al.*,[40] and Müller and Grant,[7] we employ the mechanical equilibrium equations to solve for u_{ij}^{ns} in terms of ϕ, to first order in μ/κ. The time dependence of the order parameter is assumed to obey

$$\frac{\partial\phi}{\partial t}=-\Gamma\frac{\delta\mathcal{F}}{\delta\phi}, \quad (20)$$

where the constant mobility is an inverse time scale related to the attachment and detachment kinetics of atoms at the interface evaporation-condensation mechanism for kinetics. For convenience we will set this mobility to unity hereafter (hence, time is in units of Γ^{-1}). Note that we have assumed that the main matter transport mechanism is evaporation condensation, which speeds up our simulation studies appreciably. In other words, material in the film is not conserved. While this mass-transport mode is not the dominant one for annealed films in vacuum, where the film evolves under surface diffusion, we anticipate that the physical processes we investigate in this paper are relatively insensitive to the mode of matter transport.

Defects are conserved due to their topological nature; they can only appear and disappear in pairs and hence the total Burger's vector is conserved. For b_x we have

$$\frac{\partial b_x}{\partial t}=\vec{\nabla}\cdot\vec{D}\cdot\vec{\nabla}\frac{\delta\mathcal{F}}{\delta b_x}, \quad (21)$$

where $\vec{D}$ is a mobility tensor. For simplicity we will ignore thermal noise. The relatively easy glide motion and the more sluggish motion in the climb direction,[28] have different mobilities. This is phenomenologically accounted for by writing the mobility tensor as

$$\vec{D}=\begin{pmatrix} m_g & 0 \\ 0 & m_c \end{pmatrix}, \tag{22}$$

where m_g and m_c denote the glide and climb mobilities. Note that the scalar $\Sigma_{ij}D_{i,j}a_ic_j$ formed from $\vec{D}$, say, and two arbitrary vectors $\vec{a}$ and $\vec{c}$ is invariant under reflections $x \rightarrow -x$ and $y \rightarrow y$. This implies that off-diagonal elements vanish, while the diagonal elements are arbitrary. Since vacancies are not included explicitly, we expect $m_c \ll m_g$. For thin-film growth, this is unimportant since most dislocation motion is in the climb direction in any case. We rewrite the equation of motion as

$$\frac{\partial b_x}{\partial t}=\left(m_g\frac{\partial^2}{\partial x^2}+m_c\frac{\partial^2}{\partial y^2}\right)\frac{\delta \mathcal{F}}{\delta b_x}. \tag{23}$$

The equation for b_y is of the same form with, however, $m_g\partial^2/\partial x^2+m_c\partial^2/\partial y^2 \rightarrow m_c\partial^2/\partial x^2+m_g\partial^2/\partial y^2$, in the two equations above.

Most of the functional variations of $\mathcal{F}$ can be found easily, but $\delta\mathcal{F}_{\rm coup}/\delta\phi$ is quite involved. The derivation is given in Appendix B. For the derivation, it is useful to introduce the coupling field $\beta(\vec{r})\equiv\epsilon_{ij}\delta F/\delta(\nabla_i b_j)$ between the dislocations and σ_{ij}, where ϵ_{ij} is the antisymmetric unit tensor. As discussed above, it results from integrating the strain out of the dynamics, and mediates the interaction between the defects and smooth stresses.

C. Model in the sharp-interface limit

In the absence of dislocations, one can[21] derive the following equation of motion for the film-vapor interface, as shown in Appendix C:

$$-v_n=\epsilon^2K+A\sigma_{tt}+B\sigma_{tt}^2, \tag{24}$$

where

$$A=\frac{\eta_0\epsilon^2}{2\kappa\gamma}\int dY\frac{d\phi_0}{dY}\frac{d\Phi_{\rm mis}}{d\phi_0}\Phi_{\rm mis}(\phi_0)\Phi_{\rm sol}(\phi_0), \tag{25}$$

and

$$B=\frac{4\epsilon^2}{\mu\gamma}\int dY\frac{d\phi_0}{dY}\frac{d\Phi_{\rm sol}}{d\phi_0}\Phi_{\rm mis}(\phi_0)^2. \tag{26}$$

In the above, $Y(x,y)$ is the distance normal to the curved surface at any point, $\phi_0(Y)$ is the local-equilibrium solution for the order parameter at the interface, K denotes the local curvature, $\gamma=\epsilon^2\int dY(d\phi/dY)^2$ is the surface tension, and σ_{tt} denotes the tangential stress at the interface. Furthermore, the stresses satisfy $\partial\sigma_{ij}/\partial x_j=0$, with $\sigma_{nn}=\sigma_{nt}=0$ and $\sigma_{xx}(x,y\rightarrow-\infty)=\sigma_{ext}$. Equation (24) has a transparent physical meaning: surface tension tends to flatten the interface, while larger tangential stress at the bottom of the grooves leads to faster growth, providing a positive feedback mechanism.

The presence of a nonzero deposition flux and dislocations leads to four additional terms in Eq. (24), as shown in Appendix C,

$$-v_n^{\rm net}=\epsilon^2K-\frac{H\epsilon^2}{4\gamma}+A\sigma_{tt}^{ns}+B\sigma_{tt}^{ns\,2}+C\sigma_{tt}^{s\,2}+2C\sigma_{tt}^{ns}\sigma_{tt}^{s}+\frac{\epsilon^2}{\gamma}\int dY\frac{d\phi_0}{dY}\Phi'_{\rm sol}(\nabla_x b_y-\nabla_y b_x)(\xi-\mathcal{Y}\beta), \tag{27}$$

where

$$C=-\frac{\epsilon^2}{8\gamma l^4\mathcal{Y}}\int dY\frac{d\phi_0}{dY}\Phi'_{\rm sol}Y^4. \tag{28}$$

The second term arises from deposition. For the additional three terms, two of these can be mainly attributed to dislocations in the bulk and the last one to interfacial dislocations. Both bulk and interface dislocations give rise to tangential stresses at the interface. Note that dislocations partially screen the stress giving rise to slower growth due to elasticity; furthermore, for $\sigma_{tt}^s\approx-\sigma_{tt}^{ns}$, the growth can become very slow since the net stress in the film has almost vanished. Indeed, Eq. (27) has an appealing physical interpretation. In the absence of dislocations, buckling of the surface is driven by the tangential stress at the interface. Dislocations nucleate and renormalize (screen) the stress partially. This leads to a decrease in the net σ_{tt} and hence to slower growth.

Interfacial dislocations, on the other hand, give rise to both stresses at the interface and also to the last term in Eq. (27). We can physically interpret this contribution as follows. First, in the absence of external stresses ($\beta=0$), it is straightforward to show that the above term is positive and hence favors melting of the solid. This is due to the fact that dislocations at the interface give rise to stresses in the vicinity of the interface and the system can reduce its elastic energy by eliminating these interfacial dislocations by melting. In the presence of external stresses, on the other hand, this term vanishes for

$$\xi-\mathcal{Y}\beta\approx\frac{1}{2}\frac{d^2\xi}{dY^2}Y^2-\frac{\mathcal{Y}}{2}\frac{d^2\beta}{dY^2}Y^2=-\frac{1}{2}(\sigma_{tt}^s+\sigma_{tt}^{ns})Y^2=0, \tag{29}$$

where the derivatives are evaluated at the interface, or

$$\sigma_{tt}^s=-\sigma_{tt}^{ns}. \tag{30}$$

Therefore, this term does not contribute to the evolution of the interface once the net tangential stress vanishes.

For dislocations, their dynamics in the sharp-interface limit follows from

$$\frac{\partial b_x}{\partial t}=\left[m_g\frac{\partial^2}{\partial x^2}+m_c\frac{\partial^2}{\partial y^2}\right]\left[\frac{\delta\mathcal{F}_{\rm loc}}{\delta b_x}+\mathcal{Y}\nabla_y\beta-\nabla_y\xi\right],$$

$$\frac{\partial b_y}{\partial t}=\left[m_c\frac{\partial^2}{\partial x^2}+m_g\frac{\partial^2}{\partial y^2}\right]\left[\frac{\delta\mathcal{F}_{\rm loc}}{\delta b_y}-\mathcal{Y}\nabla_x\beta+\nabla_x\xi\right], \quad (31)$$

where noise has been neglected. Since both ξ and β vanish in the vapor phase, the Burger's vector satisfies nonlinear diffusion equations, driven by $\mathcal{F}_{\rm loc}$.

In summary, our model in the sharp-interface limit reduces to three kinetic equations, namely, Eq. (27) for the film-vapor interface, Eqs. (31) for the dislocation dynamics in the solid phases, and the following equations for the auxiliary fields (ξ,β) in the solid phases:

$$\nabla^4\xi=-\mathcal{Y}(\nabla_x b_y-\nabla_y b_x) \quad (32)$$

and

$$\nabla^4\beta=\left[\frac{\delta_{ij}}{4\kappa}\nabla^2\sigma_{ij}^{ns}(\vec{r})+\frac{1}{2\mu}\left\{\varepsilon_{ik}\varepsilon_{jl}\nabla_k\nabla_l\sigma_{ij}^{ns}(\vec{r})-\frac{\delta_{ij}}{2}\nabla^2\sigma_{ij}^{ns}(\vec{r})\right\}\right]. \quad (33)$$

Finally, the boundary conditions at the interface for the elastic and auxiliary fields are $\sigma_{nn}^{ns}=\sigma_{nt}^{ns}=0$, $\xi=\vec{\nabla}\xi\cdot\vec{n}=0$, and $\beta=\vec{\nabla}\beta\cdot\vec{n}=0$. Auxiliary fields (ξ,β) are equilibrated numerically by employing an iterative method described in Appendix A.

D. Discussion

In this section we have introduced a continuum model to study the dynamics of dislocations coupled to external stresses and free surfaces in two spatial dimensions. Let us now briefly discuss some of the approximations that are employed in solving the model. For simplicity, we consider elastically isotropic systems in this paper. It is certainly true that the detailed surface structure and dislocation slip planes depend strongly on the presence of elastic and surface-tension anisotropies, as well as on the lattice structure of the film. However, the aim of this paper is to introduce a robust model that allows us to study and understand the generic features of dislocations interacting with external stresses and free surfaces at the expense of omitting various microscopic details of any particular system. On the other hand, incorporating, say, the aforementioned anisotropies is straightforward within our approach, and we envision further fruitful investigations along these lines.

While singular strains are obtained accurately by directly solving for the Airy stress function, the smooth strains are computed as a function of the order parameter from a first-order perturbative expansion in μ/κ.[7,39,40] We have verified that this approximation leads to qualitatively correct stress profiles (such as the large stress concentration at the bottom of the grooves); more accurate profiles could be obtained by including higher-order terms in the expansion, as was demonstrated recently by Hu and Chen,[36] or by directly solving the elasticity equations as was done by Kassner *et al.*[23]

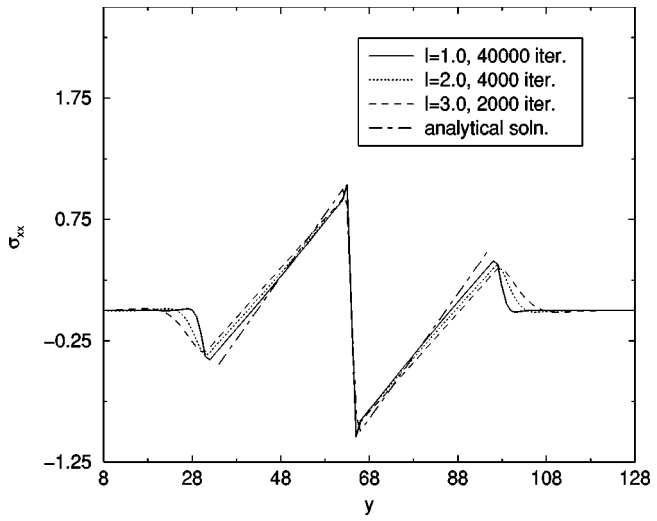

FIG. 1. Stress profiles due to a line of dislocations with varying l. Notice the convergence of σ_{xx}^{l} to the analytical result as $l/L_y\to 0$.

As the model stands now, it applies only to two-dimensional systems. In three dimensions, one must consider the topology of line defects and find a convenient way to solve the equilibrium elastic equations for the singular stresses. In Appendix D we outline how this can be achieved by employing an approach similar to that discussed in this paper.

V. RESULTS

A. Numerical studies of static dislocations

1. Convergence in quasi-one-dimensional systems

To test our approach, we have evaluated the stress component σ_{xx} in a system of dimensions $L_x=64$, $L_y=128$ due to a line of dislocations with $b_x(x,y=L_y/2)=1.0$. First, we compute ξ iteratively and then numerically evaluating $\sigma_{xx}=\partial^2\xi/\partial y^2$. The film ($\phi=1$) occupies the region $0<x<L_x$ and $32<y<96$ and is surrounded by vapor ($\phi=0$) above and below. Concerning convergence of ξ, there are two issues. First, since we employ an iterative method, we expect the solution $\xi^{n\to\infty}(l)=\xi$. Furthermore, in the limit of small l, which corresponds to enforcing effective boundary conditions at the film-vapor interface (see Appendix E), we expect $\xi^n(l)$ to approach the sharp-interface limit solution.

The results for three values of $l=(3.0,2.0,1.0)$ are shown in Fig. 1, along with an analytical solution corresponding to boundary conditions $\xi(x,y=32)=\xi(x,y=96)=0$ and $\partial\xi/\partial y(x,y=32)=\partial\xi/\partial y(x,y=96)=0$. To obtain the analytic solution, we use the Green function $G(y,y')$ satisfying

$$\frac{d^4}{dy^4}G(y,y')=\delta(y-y') \quad (34)$$

with $G(0,y')=G(L,y')=0$ and $dG(0,y')/dy=dG(L,y')/dy=0$. It is given by

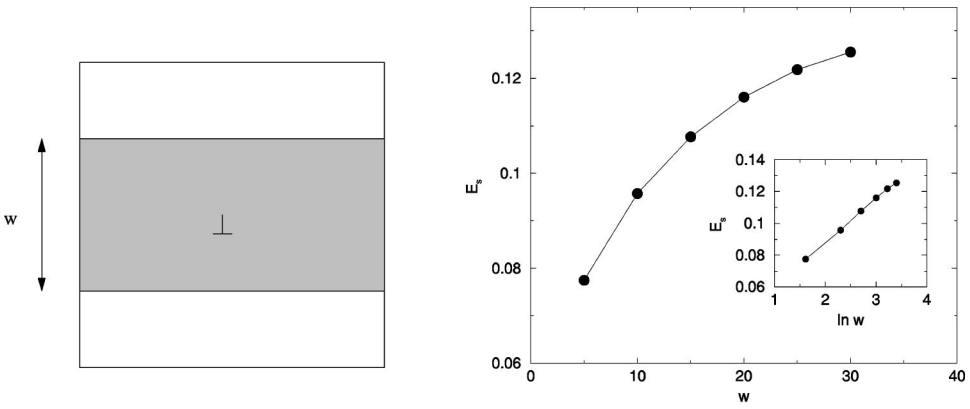

FIG. 2. Dislocation self-energy E_s as a function of film thickness w. The length of the film is $L=256$. In the inset we plot E_s vs $\ln w$, demonstrating that E_s is consistent with $E_s \propto \ln w$. The proportionality constant thus obtained is 0.027, as compared to the theoretical result of 0.02.

$$G(y,y') = \frac{1}{6}(y-y')^3\theta(y-y') + (y-y')^3\left[\frac{1}{3L^3}(L-y')^3 - \frac{1}{2L^2}(L-y')^2\right] + (y-y')^2\left[-\frac{1}{2L^2}(L-y')^3 + \frac{1}{2L}(L-y')^2\right], \tag{35}$$

where θ is the Heaviside step function. The analytical solution is built from a superposition of two $G(y,y')$ corresponding to two δ functions and σ_{xx} is evaluated from $\sigma_{xx} = d^2/dy^2[G(y,y_1)+G(y,y_2)]$.

Two things are noteworthy in the figure. First, the numerical solution converges towards the analytical result for $l/L_y \to 0$, in agreement with the sharp-interface calculation of Appendix E. Second, the number of interactions needed to converge increases rapidly in this limit. In particular, reducing l from $l=2$ to $l=1$ leads to an approximately tenfold increase in the number of iterations. Therefore, the value of l employed in simulations is dictated by two opposing considerations: first, small l is required for good convergence to the sharp-interface limit. Second, very small l will result in excessively long equilibration times. Our chosen compromise, which is physically relevant and numerically convenient, is $l=2.0$.

2. Dislocation self-energy

Consider next the numerically evaluated dislocation self-energy E_s as a function of the film thickness w, displayed in Fig. 2. Parameters used were $b_x(L_x/2,L_y/2)=1.0$, $l=2.0$, $\mu=0.25$, and $L_x=128$. This data was obtained by relaxing the auxiliary fields ξ and β to equilibrium and then evaluating

$$E_s = \int d\vec{r}\left[-\frac{1}{2\mathcal{Y}}[\nabla^2\xi(\vec{r})]^2 - \xi(\vec{r})\,\eta(\vec{r}) - \frac{1}{2\mathcal{Y}l^4}(1-\Phi_{\mathrm{sol}})\xi^2(\vec{r})\right]. \tag{36}$$

Notice the gradual increase in E_s as w is increased. Theoretically, it can be shown[30] that

$$E_s(w) \approx \frac{\mathcal{Y}b^2}{4\pi}\ln(w/b) + \text{const.} \tag{37}$$

This is due to the fact that the finite thickness of the film effectively cuts off the long-ranged singular stress fields. Plotting E_s vs $\ln w$, as shown in the inset, reveals good qualitative agreement with theory. Moreover, the numerical data gives $E_s(w) \approx 0.027 \ln w$ while the theoretical prefactor is ≈ 0.02, for this set of parameters. Hence, the prefactor is in reasonable quantitative agreement. Additionally, we have evaluated E_s for fixed w and varying b_x, and verified that $E_s \sim b_x^2$, in accord with theory. Furthermore, we find that E_s shows negligible dependence on l for $l/w \ll 1$.

3. Defect-defect interaction energy

Consider a a pair of dislocations separated by a distance d in a thin film of varying thickness $w=10,20,30$, as shown in Fig. 3. The gradient of the interaction energy E_{int} gives rise to the Peach-Koehler force discussed before. It can be shown[30] that, in an infinite system, $E_{int} \approx \text{const}(\ln d)$. Of course, a finite film thickness w cuts off long-range interactions for length scales $d \gg w$. We find that, as w is increased, E_{int} increases rapidly and reaches a plateau as d becomes comparable to $2w$. Furthermore, the plateau value E_{int}^{sat} corresponds to $E_{int}^{sat} = 2 \times E_s(w)$, as can be verified from Fig. 2, reflecting the fact that two dislocations with $d \gg w$ cease to interact. It is also clear from Fig. 3 that increasing w leads to a larger crossover length, after which the defects interact only very weakly.

4. Numerical evaluation of the critical thickness h_c

Finally, as a last test case for dislocations in static films, we demonstrate that the Matthews-Blakeslee condition for the critical thickness is correctly incorporated in the model. In the absence of external strain, $u_{ij}^{ns} \equiv 0$, the energy cost to create a defect with $|\vec{b}| = b_0$ is (including the long-range strain fields)

$$E = E_s + \frac{1}{2}E_c b_0^2, \tag{38}$$

where E_s denotes the self-energy of the defect. If, however, external strain is present, the defect-free state will be stable until

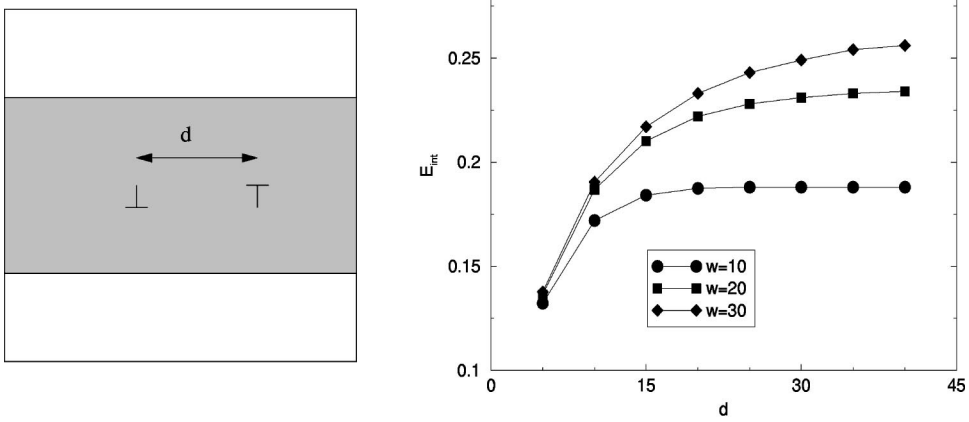

FIG. 3. Energy of interaction E_{int} for a dislocation pair in the same glide plane as a function of their separation d, for three different widths $w=10,20,30$. The length of the film is $L=256$.

$$\left| \int d\vec{r} \sum_{i,j} \sigma_{ij}^{s} u_{ij}^{ns} \right| = E. \tag{39}$$

Equation (39) is equivalent to the Matthews-Blakeslee theory of the critical thickness: Once the contribution due to external strain exceeds E, a localized defect will be nucleated. In our approach there exists a barrier separating the two free-energy minima. The height of the nucleation barrier E_n can be estimated from the local defect free energy as the barrier separating the two equal minima at $|\vec{b}|=0$ and $|\vec{b}|=b_0$; it will be of the order of the free energy at $|\vec{b}|=0.5b_0$,

$$E_n \approx \tfrac{9}{64} c\, b_0^6. \tag{40}$$

One can conveniently tune E_n by appropriately changing c while still keeping E_c and b_0 constant.

Employing similar numerical simulations to those discussed above, we computed the self-energy E_s of the dislocation as well as the interaction energy $E_{f,b}$, for misfit strain $f=0.006\,25$. This is shown in Fig. 4(a), for a symmetric film $w=2h$ with a dislocation of strength $b_x=1.0$ in the middle. This data was obtained by relaxing the auxiliary fields ξ and β to equilibrium and then evaluating

$$E_s = \int d\vec{r} \left[-\frac{1}{2\mathcal{Y}} [\nabla^2 \xi(\vec{r})]^2 - \xi(\vec{r})\,\eta(\vec{r}) - \frac{1}{2\mathcal{Y} l^4} (1-\Phi_{\rm sol}) \xi^2(\vec{r}) \right] \tag{41}$$

and

$$E_{f,b} = \int d\vec{r}\, \mathcal{Y} \eta(\vec{r}) \beta(\vec{r}). \tag{42}$$

As expected on the basis of the continuum theory, for small w, $E_s > |E_{f,b}|$ and the film remains coherent. However, for $h > h_c \approx 15$ and $E_s < |E_{f,b}|$, it is favorable for a single dislocation to nucleate. It is interesting to note that the criterion derived in Sec. II A would predict a critical thickness of $h_c \approx 10$ for the same set of parameters, a result in good agreement with our numerical estimate. In Fig. 4(b) we show similar calculations made with an asymmetric film. In particular, the lower surface was fixed at a distance $h'=32$ away from the dislocation and the upper surface was positioned at a distance h away from the dislocation. Again, the interaction energy dominates for large h, thereby giving rise to the Matthews-Blakeslee condition.

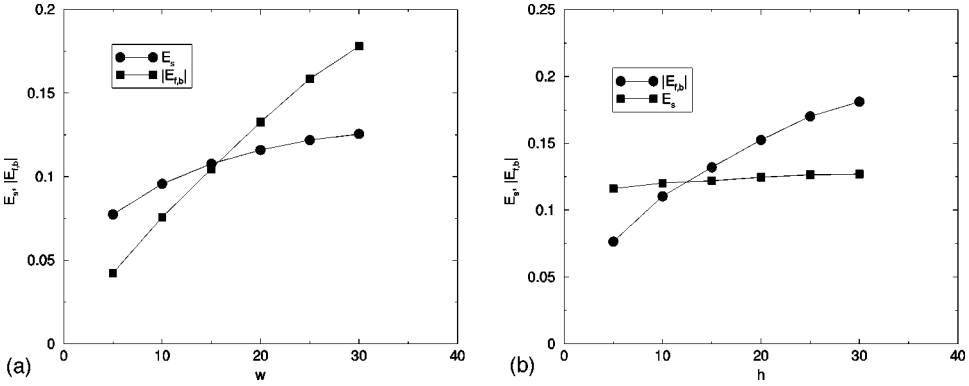

FIG. 4. (a) Numerically evaluated defect self-energy E_s and negative of the interaction energy $|E_{f,b}|$ as a function of the thickness of the symmetric film h, for misfit strain of $f=0.006\,25$. Film thickness $w=2h$, and misfit strain was applied to upper half of the system. Notice how the two curves intersect at $w_c \approx 15$, thereby favoring the nucleation of a defect for films with $w > w_c$. (b) Similar calculations in an asymmetric film. Notice how the qualitative features persist.

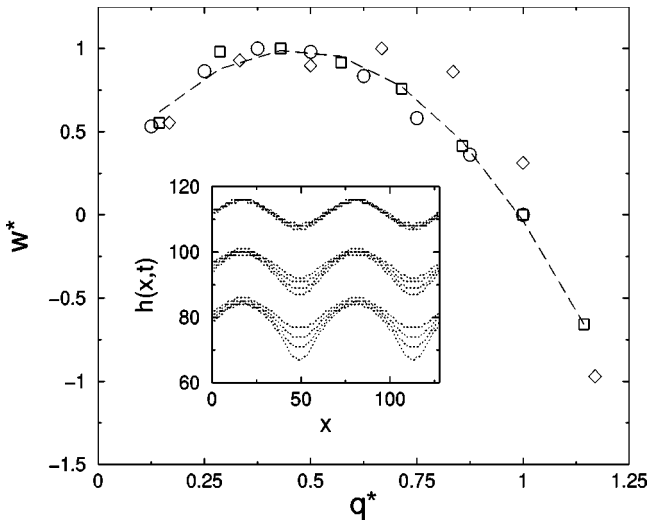

FIG. 5. Scaled amplitude of growth modes ω^* as a function of scaled wave number q^* in the early-time linearly unstable regime. Diamonds $E_c=1$, squares $E_c=50$, circles $E_c=\infty$ (no defects), dashed line is linear-stability theory. Data scaled by maximum growth rate and wave number for restabilization, both of which increase with increasing E_c. Inset shows configurations for $E_c=1,50,\infty$, from top to bottom. Four times are shown for each; grooves deepen with time for all.

B. Numerical studies of thin-film dynamics

1. Early-time regime without deposition

We have studied the early-time evolution of slightly perturbed interfaces, both with and without defects. Our results are summarized in Fig. 5, where we show interface profiles at $t=10,15,20,25$ and the growth rates of the various Fourier modes, for $E_c=1.0$, $E_c=50.0$, and $E_c=\infty$ (no defects). This data was obtained by initializing the system with a sinusoidal interface of amplitude h_0 and wave number q, and monitoring the subsequent evolution of the corresponding Fourier mode.[7] The parameters employed were $N_x\times N_y=128\times128$, $m_c=m_g=0.01$, $\mu=\eta_0=0.5$, and $\kappa=1.0$. Dislocation densities were initialized with small random fluctuations of root-mean-square magnitude 10^{-4}. At very early times ($t<10$) we observe approximately exponential growth for $h(q,t)$, as expected.[7] This phase persists longer without defects. At later times with defects, we find slower growth. Our data shows that defects decrease the initial growth rate; decreasing the defect density upon increasing E_c leads to faster growth. This can be understood from the thermodynamic theory of stressed solids by Ref. 12, according to which, for supercritical films, dislocations nucleate and anchor at the substrate-film interface thereby lowering the overall stress of the film. Qualitatively similar effects are seen upon decreasing defect mobility. In particular, reducing the mobility m_c to $m_c=0.001$ leads to practically indistinguishable results as compared to the system without defects, as far as the initial linear stability is concerned.

2. Late-time regime without deposition

In the absence of dislocations, in the nonlinear regime, the system lowers its free energy by continuously coarsening the film-vapor interface, as observed previously.[7] In Fig. 6(a) we show a typical late-time profile during the relaxation. Simulation parameters were $N_x=256$, $N_y=256$, $H=0.0$, $\mu=0.25$, $\kappa=1.0$, $\eta_0=0.775$, and $\epsilon=1.0$. The initially flat surface develops into a grooved profile with a well-defined wavelength. Eventually, the film breaks up into islands with the substrate partially exposed, in agreement with controlled annealing experiments of subcritical Si_{1-x} Ge_x films of Ozkan *et al.*[17]

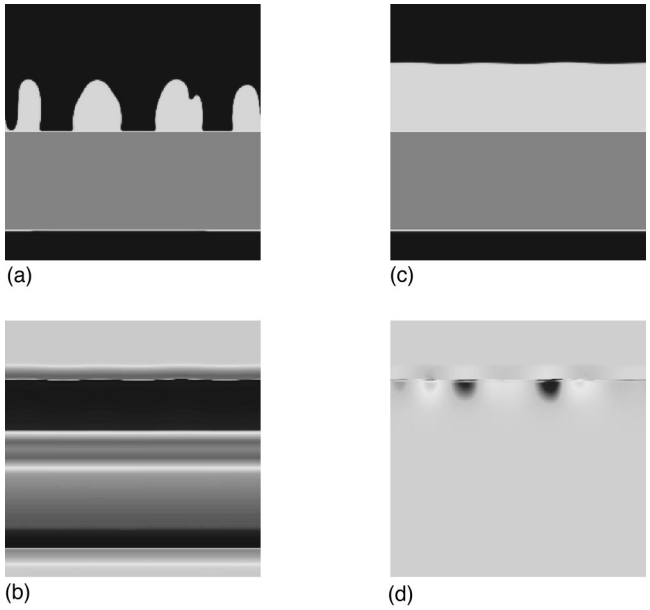

FIG. 6. (a) Typical late-time configuration for the evolving film in the absence of dislocations from a random initial condition $t=100.0$. (b) Typical late-time configuration for the evolving film with dislocations. Initial corrugation of the surface was identical to this figure, and t is the same as well. $E_c=1.0$, $m_c=m_g=0.1$, $b_0=1.0e-2$, $c_d=2.0e+6$. (c) Burger's vector x component b_x corresponding to (b). Interestingly, most of the dislocation activity in the beginning is at the film-substrate interface, in agreement with Matthews-Blakeslee theory. (d) b_y corresponding to (b).

We quantify this behavior by studying the time-dependent structure factor

$$S(q)\equiv\int dx\, e^{iqx}\langle h(x,t)h(0,t)\rangle, \tag{43}$$

as a function of wave number q, where the averaging is done over initial conditions. In Fig. 7(a) we show the structure factor at different times for a film devoid of dislocations. Simulation parameters were set to $N_x=256$, $N_y=256$, $H=0.0$, $\mu=0.25$, $\kappa=1.0$, $\eta_0=0.775$, and $\epsilon=1.0$. Notice how the peak moves to smaller wave vectors as time progresses, implying coarsening. This is illustrated in Fig. 8(a) where we plot the dominant wave vector q_{max} as time progresses, with and without defects. Analysis of $S(q)$ at earlier times reveals dynamics consistent with linearized theory. In particular, the peak of $S(q)$, S_{max}, increases approximately exponentially. The most linearly unstable wave vector dominates in the beginning, until nonlinear effects lead to competitive growth

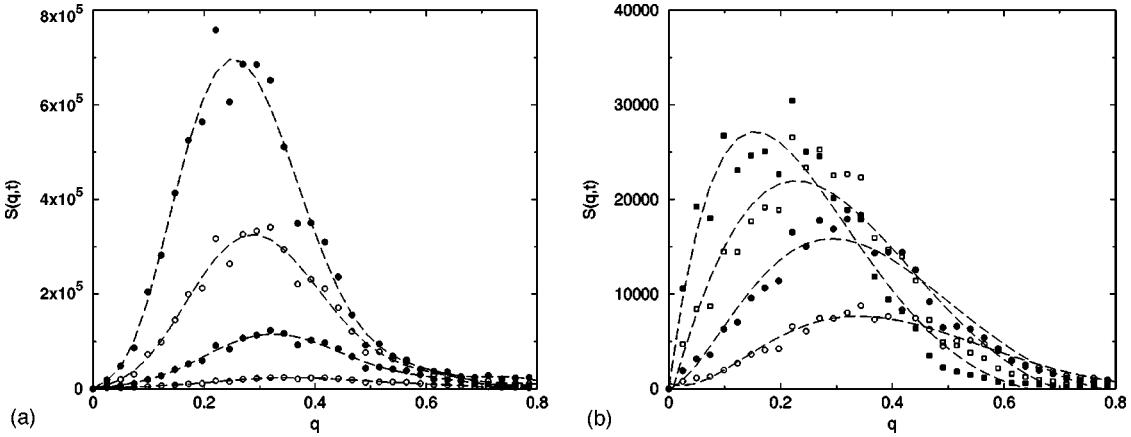

FIG. 7. (a) Time-dependent structure factor $S(q,t)$ at four different times in the absence of dislocations. From top to bottom: $t=18.0,14.0,10.0,6.0$. Dashed lines are polynomial fits to the data and serve as guides to the eye. (b) From top to bottom, $S(q,t)$ at $t=18.0,14.0,10.0,6.0$ with defects. Two things are noteworthy. First, the evolution of the morphology has slowed down considerably. Second, the most dominant wavelength occurs at smaller q when defects are present. This is a consequence of a renormalized stress in the film.

for the different modes. At later times, $S_{max} \approx A_{nd} t^{\alpha}$, with $\alpha \approx 3$, as shown in Fig. 8(b), in agreement with previous results.[7]

When dislocations are included in the dynamics, the evolution of supercritical films changes dramatically. In Fig. 6(b) we show a late-time profile starting from the *same* initial condition as in Fig. 6, with small fluctuations of average zero for the dislocation densities in the system. Simulation parameters were set to $l=2.0$, $b_0=1.0\times10^{-2}$, $c_d=2.0\times10^6$, and $m_c=m_g=0.1$. The film remains flat and the fluctuations of the solid-vapor interface become smaller at later times. This can be understood by examining the corresponding $\vec{b}$ dislocation distributions in Figs. 6(c) and 6(d). There is considerable dislocation activity at the film-substrate interface at early times. In particular, dislocations with positive b_x component of the Burgers vector align themselves at the interface. This is a consequence of the fact that the film is under tension, so positive dislocations generate a compression in the film and reduce the overall stress. Notice also how dislocations with a nonzero b_y component are located at the solid-vapor interface where σ_{xy}^{ns} and σ_{yy}^{ns} are nonzero. In particular, they are completely absent in the bulk of the film.

In general, we find that either increasing E_c or decreasing m_c (or both) leads to a more pronounced buckling and hence faster coarsening of the interface. To illustrate this, see Figs. 9(a) and 9(b) where we show a configuration with $E_c=10.0$ and $m_c=m_g=0.01$, as well as the corresponding b_x dislocation distributions. The film breaks up into islands, although the islands are somewhat larger in this case, due to the smaller effective stress in the film. Furthermore, there is a pronounced defect distribution beneath the islands, in qualitative agreement with experiments of Ozkan *et al.*[17] Physically, it is easy to see why the dislocations decouple from the system, as either $E_c \to \infty$ or $m_c \to 0$: in the first case, dislocations are energetically unfavorable in the the solid, whereas in the second case, the time for defect distribution buildup is too long, on the time scale of the buckling, to be effective in relaxing the strain.

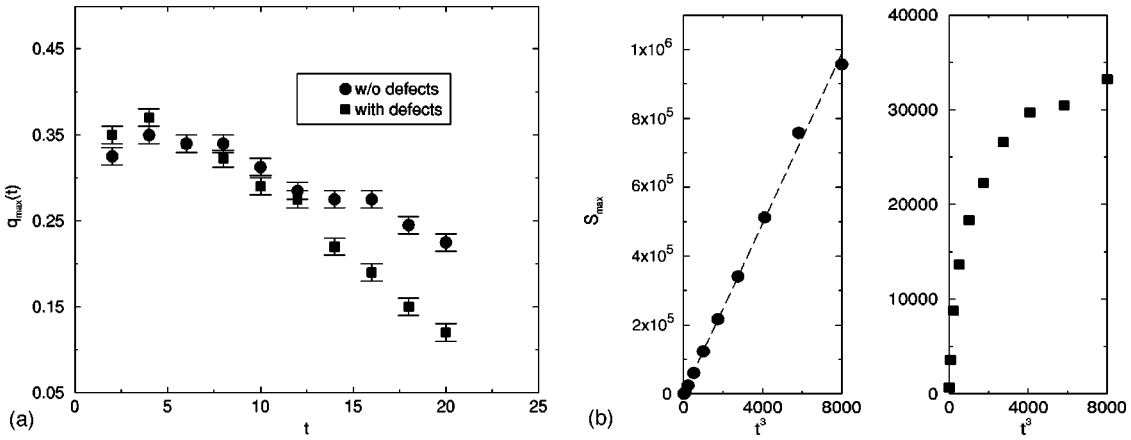

FIG. 8. (a) Time evolution of the peak position $q_{max}(t)$ both with and without dislocations. Notice how q_{max} shifts towards smaller q asymptotically with defects. (b) $S_{max}(t)$ vs t^3 at late times for both dislocated (right panel) and defect-free systems (left panel). Dashed line is a linear fit and demonstrates that the defect-free system displays behavior consistent with $S_{max}(t) \sim t^3$ at late times. Such behavior is not seen with dislocations within time scales studied here due to crossover effects.

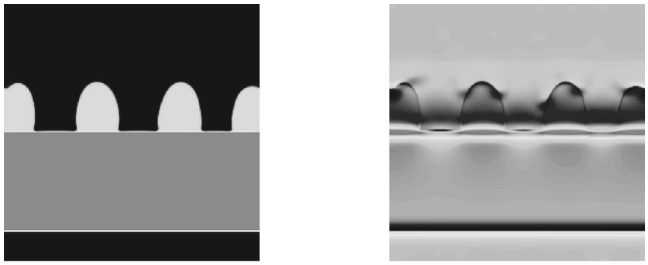

FIG. 9. (a) Typical late-time configuration for the evolving film with dislocations with large core energy and very low mobility. $E_c=10.0$, $m_c=m_g=0.01$, at $t=100.0$. (b) b_x corresponding to (a).

The behavior of $S(q,t)$, shown in Fig. 7(b), is qualitatively similar to that found in the absence of defects. Simulation parameters were set to $l=2.0$, $a=0.5$, $b_0=2.0\times10^{-2}$, $c_d=2.0\times10^6$, and $m_c=m_g=0.05$. We observe coarsening with q_{max} at smaller values of q in the nonlinear regime, as illustrated in Figs. 7(b) and 8(a). This is to be expected since the defects relax the misfit strain partially and hence the driving force for the instability is decreased. However, we do not find the asymptotic $S_{max}\sim t^{\alpha}$ as before; instead, we find a crossover to slower growth. This is illustrated in Fig. 8(b). There is a buildup of misfit dislocations in the film, which tends to slow down the growth rate, in agreement with the Matthews-Blakeslee theory.

In the asymptotic regime, where the misfit dislocations coexist with the smooth strains, the morphology of the film is determined by the strong interaction between the stress concentration at the bottom of the grooves and singular stresses.

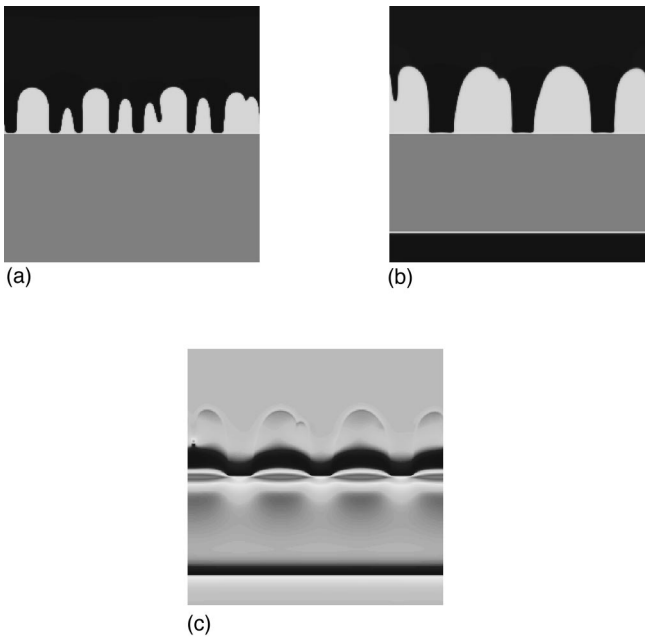

FIG. 10. (a) Typical late-time configuration for the growing film without dislocations at $t=100.0$. (b) Typical late-time configuration for the growing film with dislocations with low mobility $m_c=m_g=0.025$ and large core energy at $t=100.0$. (c) b_x corresponding to (b).

In particular, we have recently observed[27] that dislocations accumulate at the groove tips and relax the stress locally. In this regime (not observed here) we expect that $S_{max}\sim t^{\alpha}$ behavior would again be found, although there could be different behavior near the brittle-ductile transition:[27] the buildup of mobile dislocations at the groove tips in the asymptotic regime, relaxes stresses only locally, which is tantamount to renormalizing the surface tension, and hence leads to the same asymptotic behavior.

3. Late-time regime with deposition

In the presence of deposition, the morphology has a well-defined length scale, similar to the annealed films. This can be seen in Fig. 10(a) we show a profile from a simulation with nonzero deposition rate. Parameters used in this simulation were $N_x=256$, $N_y=512$, $H=0.3$, $\eta_0=3.1$, $\mu=\kappa=1.0$, and $\epsilon=1.0$. It is noteworthy, that, once the film has broken up into islands, these islands grow in the vertical direction with little coarsening in the plane of the substrate. This can be understood by recalling that the island tops are stress-free and hence preferred sites for further growth. Furthermore, it is intuitively clear that an island with height much greater than its basal width is strained only close to the substrate. Therefore, the overall length scale of the self-assembled pattern depends on the initial growth rate of the instability, deposition rate, and the initial thickness of the film. For thin enough films, the selected wavelength will be close to the most linearly unstable wavelength.

Dislocations affect the evolution of the morphology in a similar way as in the absence of deposition. In particular, mobile defects lead to a smooth interface, whereas more sluggish defects lead to a grooved profile. Furthermore, upon increasing the core energy, the film becomes more rough due to a decrease in the defect density. See Figs. 10(b) and 10(c) where order parameter and dislocation profiles are shown corresponding to $E_c=10.0$ and $m_c=0.025$. In the asymptotic regime, the film consists of islands separated by uncovered substrate. Positive dislocations become buried under the islands and there is a concentration of dislocations at indentations on the film-vapor interface, in qualitative agreement with experiments of Ozkan *et al.*[17]

VI. CONCLUSIONS AND DISCUSSION

We have introduced a nonequilibrium model of elasticity in heterogeneous systems, which includes both smooth and singular strains and their coupling to free surfaces. We have given the model a detailed exposition, as well as demonstrated that the interaction between singular and smooth stresses can lead to rich pattern-formation phenomena. In the case of annealed films, we have shown that dislocations renormalize the misfit stress in the film in agreement with Matthews-Blakeskee theory. Moreover, we have shown that the film undergoes a buckling instability, driven by the residual stress in the film. We have quantified this by numerically evaluating the linear dispersion relation $\omega(q)$. In particular, we have shown that increasing core energy and

decreasing mobility lead to less effective screening of the external stress. Furthermore, we have recently shown[27] that dislocations interact very strongly with the smooth stresses in the nonlinear regime. This is due to the stress concentration at the bottom of the grooves. A deeper understanding of the physics in the asymptotic regime requires unraveling the coupled dynamics of dislocations and stress concentration at the bottom of the grooves. This will be addressed in a separate publication.

So far as films with deposition are concerned, we have shown that (i) in the absence of dislocations, the film breaks up into islands with a well-defined length scale, in qualitative agreement with experiments, and (ii) dislocations affect the morphology through strain relaxation. In particular, in the presence of mobile dislocations, the film-vapor interface remains smooth. However, upon decreasing the number or the mobility of dislocations leads to more rough morphologies. Finally, we note that the qualitative features reported above are robust towards varying the elastic parameters. In particular, we have varied l, E_c, η_0, and μ and found qualitatively similar behavior.

It would be of interest to extend this approach to three spatial dimensions; an outline for the procedure is given in Appendix D. In particular, this would enable one to study the detailed interactions between defects and smooth strains in experimentally relevant situations.

ACKNOWLEDGMENTS

This work was supported by the Natural Sciences and Engineering Research Council of Canada, le Fonds pour la Formation de Chercheurs et l'Aide à la Recherche du Québec, and, in part, by the Academy of Finland (M.H.). We thank Mohsen Sabouri-Ghomi, Nick Provatas, Martin Dubé, and Ken Elder for useful discussions.

APPENDIX A: EQUILIBRATION OF THE AUXILIARY FIELDS (ξ,β)

The equations of motion, Eqs. (20) and (21), together with Eqs. (19) that determine the quasistatic fields (ξ,β), completely specify the dynamics of the model. The fields (ξ,β) were equilibrated every nth iteration using an iterative spectral method. Typically, $n=10$–30. It was verified that decreasing n did not affect the results reported in this paper. The main idea of this method is as follows. Since the biharmonic equation with constant coefficients is diagonal in Fourier space and hence amenable to fast numerical solution using the fast Fourier transform (FFT) method, one obtains the following scheme: First, an initial solution $\xi^0_{i,j}$ is obtained. Then, if $\xi=\delta\xi+\xi^0$ is a solution, it follows that $\delta\xi$ satisfies

$$\frac{1}{\mathcal{Y}}\nabla^4\delta\xi+\frac{1}{\mathcal{Y}l^4}(1-\Phi_{\rm sol})\,\delta\xi = -\eta-\frac{1}{\mathcal{Y}}\nabla^4\xi^0+1/(\mathcal{Y}l^4)(1-\Phi_{\rm sol})\xi^0. \quad \text{(A1)}$$

We obtain an approximate solution $\delta\tilde{\xi}$ by taking the spatial average of $1/(\mathcal{Y}l^4)(1-\Phi_{\rm sol})$, and solving the resulting biharmonic equation with FFT. A new approximation ξ^1 is obtained from

$$\xi^1=\xi^0+0.15\delta\tilde{\xi}. \quad \text{(A2)}$$

The new correction is obtained by solving

$$\frac{1}{\mathcal{Y}}\nabla^4\delta\tilde{\xi}+\lambda_{eff}^{-4}\delta\tilde{\xi}=-\eta-\frac{1}{\mathcal{Y}}\nabla^4\xi^1+1/(\mathcal{Y}l^4)(1-\Phi_{\rm sol})\xi^1, \quad \text{(A3)}$$

where $L_xL_y\lambda_{eff}^{-4}\equiv\int d\vec{r}\,1/(\mathcal{Y}l^4)(1-\Phi_{\rm sol})$. This process is repeated until the magnitude of the correction $|\delta\tilde{\xi}|$ is less than the preset tolerance $\epsilon_{tol}=3.0\times10^{-5}$. Typically, this corresponds to approximately 100 successive iterations of Eqs. (A2) and (A3).

Furthermore, Eqs. (19) are relaxed dynamically after each time step with 50 Euler iterations. Finally, the phase field ϕ and dislocation densities (b_x,b_y) are updated using finite differencing for the spatial gradients and the Euler method for time evolution. Typical system sizes used in this study were $N_x\times N_y=64\times128$ to 512×512. Typical values for the parameters were $\Delta x=1.0$, $\Delta t=0.01$, $\epsilon=\Delta x=1.0$, $m_g=1.0$, $m_c=1.0-0.0001$, $E_c=10.0-0.01$, $c_d=200.0$, $b_0=0.1$, $l=2.0$, $b_0=0.1$, $N_{skip}=10$. We also verified that a smaller $dt=0.005$ and $N_{skip}=5$ led to identical results.

APPENDIX B: ORDER-PARAMETER AND FUNCTIONAL DERIVATIVES

Most of the terms in Eq. (3) can be used in a straightforward manner to work out the functional derivatives with respect to the relevant fields (ϕ,b_x,b_y) for the equations of motion. The exception is $\mathcal{F}_{\rm coup}$.

1. Dislocation density

The coupling in terms of the Airy stress function χ is

$$\mathcal{F}_{\rm coup}=-\int d\vec{r}\,\sigma_{ij}^{ns}\left[\frac{\delta_{ij}}{4\kappa}\nabla^2\chi+\frac{1}{2\mu}\left(\varepsilon_{ik}\varepsilon_{jl}\nabla_k\nabla_l\chi-\frac{\delta_{ij}}{2}\nabla^2\chi\right)\right], \quad \text{(B1)}$$

where we have employed Hooke's law to express strains in terms of stresses and hence the Airy stress function χ.

Let the Green function $G(\vec{r},\vec{r}')$ satisfy

$$\nabla^4G(\vec{r},\vec{r}')+l^{-4}(1-\Phi_{\rm sol})G(\vec{r},\vec{r}')=\delta(\vec{r}-\vec{r}'). \quad \text{(B2)}$$

The formal solution of Eq. (17) is thus

$$\chi(\vec{r})=\mathcal{Y}\int d\vec{r}'\,G(\vec{r},\vec{r}')\Phi_{\rm sol}[\phi(\vec{r}')](\nabla'_xb_y-\nabla'_yb_x) =\mathcal{Y}\int d\vec{r}'\,G(\vec{r},\vec{r}')\,\eta(\vec{r}'). \quad \text{(B3)}$$

This allows us to rewrite Eq. (B1) as

$$\mathcal{F}_{\rm coup}=\int d\vec{r}\,\sigma_{ij}^{ns}\int d\vec{r}'\left[\frac{\delta_{ij}}{4\kappa}\nabla^2 G(\vec{r},\vec{r}')\mathcal{Y}\eta(\vec{r}')+\frac{1}{2\mu}\left\{\varepsilon_{ik}\varepsilon_{jl}\nabla_k\nabla_l G(\vec{r},\vec{r}')\mathcal{Y}\eta(\vec{r}')-\frac{\delta_{ij}}{2}\nabla^2 G(\vec{r},\vec{r}')\mathcal{Y}\eta(\vec{r}')\right\}\right]$$
$$=\int d\vec{r}'\,\mathcal{Y}\eta(\vec{r}')\int d\vec{r}\,\sigma_{ij}^{ns}\left[\frac{\delta_{ij}}{4\kappa}\nabla^2 G(\vec{r},\vec{r}')+\frac{1}{2\mu}\left\{\varepsilon_{ik}\varepsilon_{jl}\nabla_k\nabla_l G(\vec{r},\vec{r}')-\frac{\delta_{ij}}{2}\nabla^2 G(\vec{r},\vec{r}')\right\}\right]. \tag{B4}$$

Upon interchanging $\vec{r}$ and $\vec{r}'$ and carrying out two partial integrations one finally arrives at (note that surface terms vanish due to periodic boundary conditions)

$$\mathcal{F}_{\rm coup}=\int d\vec{r}\,\mathcal{Y}\eta(\vec{r})\int d\vec{r}'\,G(\vec{r},\vec{r}')\left[\frac{\delta_{ij}}{4\kappa}\nabla'^2\sigma_{ij}^{ns}(\vec{r}')+\frac{1}{2\mu}\left\{\varepsilon_{ik}\varepsilon_{jl}\nabla_k'\nabla_l'\sigma_{ij}^{ns}(\vec{r}')-\frac{\delta_{ij}}{2}\nabla'^2\sigma_{ij}^{ns}(\vec{r}')\right\}\right]$$
$$\equiv\int d\vec{r}\,\mathcal{Y}\eta(\vec{r})\beta(\vec{r}), \tag{B5}$$

where

$$\beta(\vec{r})\equiv\int d\vec{r}'\,G(\vec{r},\vec{r}')\left[\frac{\delta_{ij}}{4\kappa}\nabla'^2\sigma_{ij}^{ns}(\vec{r}')+\frac{1}{2\mu}\left\{\varepsilon_{ik}\varepsilon_{jl}\nabla_k'\nabla_l'\sigma_{ij}^{ns}(\vec{r}')-\frac{\delta_{ij}}{2}\nabla'^2\sigma_{ij}^{ns}(\vec{r}')\right\}\right]. \tag{B6}$$

Since we do not have a closed-form expression for G, we evaluate β numerically in a similar manner as ξ,

$$\nabla^4\beta(\vec{r})+l^{-4}(1-\Phi_{\rm sol})\beta(\vec{r})=\left[\frac{\delta_{ij}}{4\kappa}\nabla^2\sigma_{ij}^{ns}(\vec{r})+\frac{1}{2\mu}\left\{\varepsilon_{ik}\varepsilon_{jl}\nabla_k\nabla_l\sigma_{ij}^{ns}(\vec{r})-\frac{\delta_{ij}}{2}\nabla^2\sigma_{ij}^{ns}(\vec{r})\right\}\right]. \tag{B7}$$

The asymptotic solution for β is given by Eq. (B6). Hence, with this formulation the dynamics from the coupling to external stresses for the $b_{x,y}$ fields are straightforward to calculate.

2. Order parameter

In order to treat ϕ, we proceed as follows. First, we rewrite $\mathcal{F}_{\rm coup}$ (after two partial integrations) as

$$\mathcal{F}_{\rm coup}=\int d\vec{r}\,\chi(\vec{r})\left[\frac{\delta_{ij}}{4\kappa}\nabla^2\sigma_{ij}^{ns}(\vec{r})+\frac{1}{2\mu}\left\{\varepsilon_{ik}\varepsilon_{jl}\nabla_k\nabla_l\sigma_{ij}^{ns}(\vec{r})-\frac{\delta_{ij}}{2}\nabla^2\sigma_{ij}^{ns}(\vec{r})\right\}\right]. \tag{B8}$$

Hence,

$$\frac{\delta\mathcal{F}_{\rm coup}}{\delta\phi(\vec{r})}=\int d\vec{r}'\frac{\delta\mathcal{F}_{\rm coup}}{\delta\chi(\vec{r}')}\frac{\delta\chi(\vec{r}')}{\delta\phi(\vec{r})}=\int d\vec{r}'\left[\frac{\delta_{ij}}{4\kappa}\nabla'^2\sigma_{ij}^{ns}+\frac{1}{2\mu}\left\{\varepsilon_{ik}\varepsilon_{jl}\nabla_k'\nabla_l'\sigma_{ij}^{ns}-\frac{\delta_{ij}}{2}\nabla'^2\sigma_{ij}^{ns}\right\}\right]\frac{\delta\chi(\vec{r}')}{\delta\phi(\vec{r})}. \tag{B9}$$

Furthermore, since χ satisfies

$$\nabla'^4\chi(\vec{r}')+\frac{(1-\Phi_{\rm sol})}{l^4}\chi(\vec{r}')=\mathcal{Y}\Phi_{\rm sol}(\vec{r}')(\nabla_x'b_y-\nabla_y'b_x), \tag{B10}$$

it follows that

$$\nabla'^4\frac{\delta\chi(\vec{r}')}{\delta\phi(\vec{r})}+l^{-4}[1-\Phi_{\rm sol}(\vec{r}')]\frac{\delta\chi(\vec{r}')}{\delta\phi(\vec{r})}=\mathcal{Y}\frac{\delta\Phi_{\rm sol}(\vec{r}')}{\delta\phi(\vec{r})}(\nabla_x'b_y-\nabla_y'b_x)+l^{-4}\frac{\delta\Phi_{\rm sol}(\vec{r}')}{\delta\phi(\vec{r})}\chi(\vec{r}'). \tag{B11}$$

The formal solution of Eq. (B11) can be written as

$$\frac{\delta\chi(\vec{r}')}{\delta\phi(\vec{r})}=\int d\vec{r}''G(\vec{r}',\vec{r}'')\left[\mathcal{Y}\frac{\delta\Phi_{\rm sol}(\vec{r}'')}{\delta\phi(\vec{r})}(\nabla_x''b_y-\nabla_y''b_x)+\frac{1}{l^4}\frac{\delta\Phi_{\rm sol}(\vec{r}'')}{\delta\phi(\vec{r})}\chi(\vec{r}'')\right]. \tag{B12}$$

However, since $\delta\Phi_{\rm sol}(\vec{r}'')/\delta\phi(\vec{r})=\Phi_{\rm sol}'(\vec{r}'')\delta(\vec{r}-\vec{r}'')$, it follows that

$$\frac{\delta\chi(\vec{r}')}{\delta\phi(\vec{r})}=G(\vec{r},\vec{r}')\times\left(\mathcal{Y}\Phi_{\rm sol}'(\vec{r})(\nabla_x b_y-\nabla_y b_x)+\frac{1}{l^4}\Phi_{\rm sol}'(\vec{r})\chi(\vec{r})\right). \tag{B13}$$

Substituting this in Eq. (B9) finally yields

$$\frac{\delta \mathcal{F}_{\rm coup}}{\delta \phi(\vec{r})} = \left(\mathcal{Y}\Phi'_{\rm sol}(\vec{r})(\nabla_x b_y - \nabla_y b_x) + \frac{1}{l^4}\Phi'_{\rm sol}(\vec{r})\chi(\vec{r}) \right) \times \int d\vec{r}\,' G(\vec{r},\vec{r}\,') \left[\frac{\delta_{ij}}{4\kappa}\nabla'^2 \sigma^{ns}_{ij} + \frac{1}{2\mu}\left(\varepsilon_{ik}\varepsilon_{jl}\nabla'_k\nabla'_l\sigma^{ns}_{ij} - \frac{\delta_{ij}}{2}\nabla'^2\sigma^{ns}_{ij} \right) \right] \equiv \left(\mathcal{Y}\Phi'_{\rm sol}(\vec{r})(\nabla_x b_y - \nabla_y b_x) + \frac{1}{l^4}\Phi'_{\rm sol}(\vec{r})\chi(\vec{r}) \right)\beta(\vec{r}). \tag{B14}$$

As a final step, we replace χ by $-\xi$ and obtain

$$\frac{\delta \mathcal{F}_{\rm coup}}{\delta \phi(\vec{r})} = \left(\mathcal{Y}\Phi'_{\rm sol}(\vec{r})(\boldsymbol{\nabla}_x b_y - \boldsymbol{\nabla}_y b_x) - \frac{1}{l^4}\Phi'_{\rm sol}(\vec{r})\xi(\vec{r}) \right)\beta(\vec{r}). \tag{B15}$$

The remaining functional derivatives are straightforward to obtain. For completeness, we list all such derivatives below.

$$\frac{\delta \mathcal{F}_{\phi}}{\delta \phi} = -l^2\nabla^2\phi + f_{\phi} + \frac{\eta_0^2}{\kappa}\Phi_{\rm mis}\Phi'_{\rm mis},$$

$$\frac{\delta \mathcal{F}_{\rm ext}}{\delta \phi} = \eta_0 \Phi'_{\rm mis}\vec{\nabla}\cdot\vec{u}^{ns},$$

$$\frac{\delta \mathcal{F}_{\rm el}}{\delta \phi} = \mu\Phi'_{\rm sol}\sum_{i,j}\left(u^{ns}_{ij} - \frac{\delta_{ij}}{d}\nabla\cdot\vec{u}^{ns} \right)^2,$$

$$\frac{\delta \mathcal{F}_{\rm int}}{\delta \phi} = \frac{1}{2\mathcal{Y}l^4}\Phi'_{\rm sol}\xi^2 - \xi\Phi'_{\rm sol}(\nabla_x b_y - \nabla_y b_x),$$

$$\frac{\delta \mathcal{F}_{\rm coup}}{\delta \phi} = \left(\mathcal{Y}\Phi'_{\rm sol}(\nabla_x b_y - \nabla_y b_x) - \frac{1}{l^4}\Phi'_{\rm sol}\xi(\vec{r}) \right)\beta(\vec{r}),$$

$$\frac{\delta \mathcal{F}_{\rm int}}{\delta \xi(\vec{r})} = \frac{1}{\mathcal{Y}}\nabla^4\xi + \eta + \frac{1}{\mathcal{Y}l^4}(1-\Phi_{\rm sol})\xi,$$

$$\frac{\delta \mathcal{F}_{\rm coup}}{\delta \xi} = 0,$$

$$\frac{\delta \mathcal{F}_{\rm int}}{\delta b_x(\vec{r})} = -\nabla_y(\xi\,\Phi_{\rm sol}),$$

$$\frac{\delta \mathcal{F}_{\rm loc}}{\delta b_x} = 2c\,b_x[(\vec{b}^2 - b_0^2)^2 + 2\vec{b}^2(\vec{b}^2 - b_0^2)] + 2E_c b_x,$$

$$\frac{\delta \mathcal{F}_{\rm coup}}{\delta b_x} = \mathcal{Y}\nabla_y[\Phi_{\rm sol}\beta(\vec{r})],$$

$$\frac{\delta \mathcal{F}_{\rm int}}{\delta b_y(\vec{r})} = \nabla_x(\xi\,\Phi_{\rm sol}),$$

$$\frac{\delta \mathcal{F}_{\rm loc}}{\delta b_y} = 2c\,b_y[(\vec{b}^2 - b_0^2)^2 + 2\vec{b}^2(\vec{b}^2 - b_0^2)] + 2E_c b_y,$$

$$\frac{\delta \mathcal{F}_{\rm coup}}{\delta b_y} = -\mathcal{Y}\nabla_x[\Phi_{\rm sol}\beta(\vec{r})],$$

$$\frac{\delta \mathcal{F}_{\rm flux}}{\delta \phi} = -j(\vec{r})(\phi - \phi^3). \tag{B16}$$

APPENDIX C: INTERFACE EQUATION OF MOTION IN THE SHARP-INTERFACE LIMIT

In this Appendix we will derive the equation of motion for the solid-liquid interface by employing the projection-operator method, valid in the thin interface limit $K\epsilon \ll 1$, where K denotes the local curvature of the interface and ϵ is the width of the diffuse interface.

We begin by writing down the equation of motion for the order parameter ϕ

$$\frac{\partial \phi}{\partial t} = \frac{\epsilon^2}{2}\nabla^2\phi - \frac{1}{a}\frac{df(\phi)}{d\phi} + H\frac{dg}{d\phi} - \frac{\eta_0^2}{\kappa}\frac{d\Phi_{\rm mis}}{d\phi}\Phi_{\rm mis} - \eta_0\frac{d\Phi_{\rm mis}}{d\phi}\vec{\nabla}\cdot\vec{u} - \mu\frac{d\Phi_{\rm sol}}{d\phi}\sum_{ij}\left(u_{ij} - \frac{\delta_{ij}}{2}\vec{\nabla}\cdot\vec{u} \right)^2. \tag{C1}$$

We use an orthogonal coordinate system (X,Y), where $Y(x,y)$ denotes the distance to the interface from point (x,y) along a normal to the interface, and $X(x,y)$ denotes the arc length along the interface measured from some reference point. We define the interface position to be given by the level set $\phi = 1/2$.

Next, given a gently curved interface on the scale of ϵ, we write the solution to Eq. (C1) in the quasistationary approximation as

$$\phi(\vec{r},t) \approx \phi_0(w(\vec{r},t)), \tag{C2}$$

where ϕ_0 satisfies

$$\epsilon^2\frac{d^2\phi_0}{dY^2} - \frac{1}{a}\frac{df(\phi_0)}{d\phi_0} = 0, \tag{C3}$$

with

$$\lim_{Y\to\infty}\phi_0 = 0; \quad \lim_{Y\to-\infty}\phi_0 = 1. \tag{C4}$$

Furthermore, the Laplacian in the new coordinate system becomes

$$\nabla^2=\frac{\partial^2}{\partial Y^2}+\frac{K}{1+YK}\frac{\partial}{\partial Y}+(1+YK)^2\frac{\partial^2}{\partial X^2}+3(1+YK)Y\frac{\partial K}{\partial X}\frac{\partial}{\partial X}. \tag{C5}$$

However, in the vicinity of the interface ($Y=0$), the Laplacian can be approximated by

$$\nabla^2\approx\frac{\partial^2}{\partial Y^2}+K\frac{\partial}{\partial Y}+\frac{\partial^2}{\partial X^2}. \tag{C6}$$

Hence, the equation of motion can be written as

$$\frac{d\phi_0}{dY}\frac{\partial Y}{\partial t}=\epsilon^2\frac{d^2\phi_0}{dY^2}+\epsilon^2K\frac{d\phi_0}{dY}-\frac{1}{a}\frac{df(\phi)}{d\phi}+H\frac{dg}{d\phi}-\frac{\eta_0^2}{\kappa}\frac{d\Phi_{\rm mis}}{d\phi}\Phi_{\rm mis}-\eta_0\frac{d\Phi_{\rm sol}}{d\phi}\vec{\nabla}\cdot\vec{u}-\mu\frac{dg(\phi)}{d\phi}\sum_{ij}\left(u_{ij}-\frac{\delta_{ij}}{2}\vec{\nabla}\cdot\vec{u}\right)^2, \tag{C7}$$

which, by virtue of Eq. (C3), becomes

$$\frac{d\phi_0}{dY}\frac{\partial Y}{\partial t}=\epsilon^2K\frac{d\phi_0}{dY}-\frac{\eta_0^2}{\kappa}\frac{d\Phi_{\rm mis}}{d\phi}\Phi_{\rm mis}+H\frac{dg}{d\phi}-\eta_0\frac{d\Phi_{\rm mis}}{d\phi}\vec{\nabla}\cdot\vec{u}-\mu\frac{d\Phi_{\rm sol}}{d\phi}\sum_{ij}\left(u_{ij}-\frac{\delta_{ij}}{2}\vec{\nabla}\cdot\vec{u}\right)^2. \tag{C8}$$

In order to project the bulk dynamics onto the interface, we multiply both sides of Eq. (C8) by $d\phi_0/dY$, and integrate over Y over the whole domain

$$\frac{\partial Y}{\partial t}\int dY\left(\frac{d\phi_0}{dY}\right)^2=\epsilon^2K\int dY\left(\frac{d\phi_0}{dY}\right)^2+H\int dY\frac{d\phi_0}{dY}\frac{dg}{d\phi}-\int dY\frac{d\phi_0}{dY}\times\left[\frac{\eta_0^2}{\kappa}\frac{d\Phi_{\rm mis}}{d\phi}\Phi_{\rm mis}+\eta_0\frac{d\Phi_{\rm mis}}{d\phi}\vec{\nabla}\cdot\vec{u}+\mu\frac{d\Phi_{\rm sol}}{d\phi}\sum_{ij}\left(u_{ij}-\frac{\delta_{ij}}{2}\vec{\nabla}\cdot\vec{u}\right)^2\right]. \tag{C9}$$

In passing, we note that

$$\int dY\frac{d\phi_0}{dY}=-1, \tag{C10}$$

and

$$\gamma=\int dY\left[\frac{\epsilon^2}{2}\left(\frac{d\phi_0}{dY}\right)^2+\frac{1}{a}f(\phi_0)\right]=\frac{7\sqrt{2}}{60}\frac{\epsilon}{\sqrt{a}}, \tag{C11}$$

is the surface tension. This result can be readily derived as follows. First, from Eq. (C3) it follows that

$$\frac{\epsilon^2}{2}\left(\frac{d\phi_0}{dY}\right)^2=\frac{1}{a}f(\phi_0), \tag{C12}$$

and, therefore,

$$\gamma=\int dY\epsilon^2\left(\frac{d\phi_0}{dY}\right)^2=\int_1^0 d\phi_0\epsilon^2\frac{d\phi_0}{dY}. \tag{C13}$$

Furthermore, from Eq. (C12) it follows that

$$\frac{d\phi_0}{dY}=-\sqrt{\frac{2}{a\epsilon^2}}\phi_0^2(\phi_0-1)(\phi_0-2), \tag{C14}$$

for our choice of $f=\phi^4(\phi-1)^2(\phi-2)^2$. Upon substituting Eq. (C14) in Eq. (C13) yields Eq. (C11).

Returning to the equation of motion, from Eq. (C9) we obtain

$$-v_n=\epsilon^2K+\frac{\epsilon^2H}{\gamma}\int dY\frac{d\phi_0}{dY}\frac{dg}{d\phi}-\frac{\epsilon^2}{\gamma}\int dY\frac{d\phi_0}{dY}\left[\frac{\eta_0^2}{\kappa}\frac{d\Phi_{\rm mis}}{d\phi}\Phi_{\rm mis}+\eta_0\frac{d\Phi_{\rm mis}}{d\phi}\vec{\nabla}\cdot\vec{u}+\mu\frac{d\Phi_{\rm sol}}{d\phi}\sum_{ij}\left(u_{ij}-\frac{\delta_{ij}}{2}\vec{\nabla}\cdot\vec{u}\right)^2\right]. \tag{C15}$$

Next we wish to express the strains in terms of the stresses, by employing the definition of the stress

$$\vec{\nabla}\cdot\vec{u}=\frac{1}{\kappa}\left(\frac{\sigma_{ii}}{2}-\eta_0\Phi_{\rm mis}(\phi_0)\right), \tag{C16}$$

and

$$u_{ij}-\frac{\delta_{ij}}{2}\vec{\nabla}\cdot\vec{u}=\frac{1}{2\mu\Phi_{\rm sol}(\phi_0)}\left(\sigma_{ij}-\frac{1}{2}\sigma_{ii}\delta_{ij}\right). \tag{C17}$$

Therefore, the equation of motion for the interface is

$$-v_n=\epsilon^2K-\frac{H\epsilon^2}{4\gamma}-\frac{\epsilon^2}{\gamma}\int dY\frac{d\phi_0}{dY}\left[\frac{\eta_0}{2\kappa}\frac{d\Phi_{\rm mis}}{d\phi}\sigma_{ll}+\frac{1}{4\mu\Phi_{\rm sol}(\phi_0)^2}\frac{d\Phi_{\rm sol}}{d\phi}\sum_{ij}\left(\sigma_{ij}-\frac{1}{2}\sigma_{ii}\delta_{ij}\right)^2\right]. \tag{C18}$$

Since $d\phi_0/dY$ is sharply peaked at the interface, the integral in Eq. (C18) is nonzero only at the interface. Also, since force balance across the interface requires $\sigma_{nn}=\sigma_{nt}=0$ (liquid is assumed to have negligible pressure), this implies that σ_{tt} is constant along the interface in order to preserve mechanical equilibrium close to the interface. Furthermore, employing the known spatial dependence of the planar solution for the stresses we may write

$$\sigma_{tt}=\tilde{\sigma}_{tt}\Phi_{\rm mis}(\phi_0)\Phi_{\rm sol}(\phi_0), \tag{C19}$$

where $\tilde{\sigma}_{tt}$ denotes the magnitude of σ_{tt}. Hence, we arrive at

$$-v_n=\epsilon^2K-\frac{H\epsilon^2}{4\gamma}+A\tilde{\sigma}_{tt}+B\tilde{\sigma}_{tt}^2, \tag{C20}$$

where

$$A=\frac{\eta_0\epsilon^2}{2\kappa\gamma}\int dY\frac{d\phi_0}{dY}\frac{d\Phi_{\rm mis}}{d\phi_0}\Phi_{\rm mis}(\phi_0)\Phi_{\rm sol}(\phi_0) \tag{C21}$$

and

$$B=\frac{4\epsilon^2}{\mu\gamma}\int dY\frac{d\phi_0}{dY}\frac{d\Phi_{\rm sol}}{d\phi_0}\Phi_{\rm mis}(\phi_0)^2. \tag{C22}$$

Notice that this equation is nonlocal due to the mechanical equilibrium condition $\vec{\nabla}\cdot\vec{\sigma}=0$ that gives rise to σ_{tt}.

1. Interface dynamics with defects

When defects are included, there are additional terms in the interface equation of motion. To this end, we write the local velocity of the interface as

$$v_n^{\rm net}=v_n+(\delta v)_n^b+(\delta v)_n^i, \tag{C23}$$

where v_n denotes the velocity in the absence of defects [see Eq. (C20)], and $(\delta v)_n^b$ and $(\delta v)_n^i$ arise from bulk and interfacial dislocations, respectively. Consider bulk defects. In this case it is easy to show that there are two additional terms that can be written as

$$-(\delta v)_n^b=-\frac{\epsilon^2}{2\gamma l^4}\int dY\frac{d\phi_0}{dY}\left(\frac{1}{\mathcal{Y}}\Phi'_{\rm sol}\xi^2-2\Phi'_{\rm sol}\xi\beta\right). \tag{C24}$$

Now, using the fact that, in the sharp interface limit, $\xi=d\xi/dn=0$ and $\beta=d\beta/dn=0$, at the interface, we can make a Taylor expansion and write

$$\xi\approx\frac{1}{2}\frac{d^2\xi}{dY^2}Y^2+\cdots, \tag{C25}$$

and

$$\beta\approx\frac{1}{2}\frac{d^2\beta}{dY^2}Y^2+\cdots, \tag{C26}$$

where the derivatives are evaluated at the interface. Now, we note that the singular component of the tangential stress at the interface σ_{tt}^s is given by $-d^2\xi/dY^2$. Furthermore, upon employing the definition of β and recalling that, in the vicinity of the interface, $\sigma_{nn}^{ns}=\sigma_{nt}^{ns}=0$, we find that at the interface $\sigma_{tt}^{ns}/\mathcal{Y}\approx d^2\beta/dY^2$. With this insight we can rewrite Eq. (C23) as

$$-v_n^{\rm net}=\epsilon^2K-\frac{H\epsilon^2}{4\gamma}+A\sigma_{tt}^{ns}+B\,\sigma_{tt}^{ns\,2}+C\,\sigma_{tt}^{s\,2}+2\,C\,\sigma_{tt}^{ns}\sigma_{tt}^s-(\delta v)_n^i, \tag{C27}$$

where

$$C=-\frac{\epsilon^2}{8\gamma l^4\mathcal{Y}}\int dY\frac{d\phi_0}{dY}\Phi'_{\rm sol}Y^4. \tag{C28}$$

Finally, let us consider the contribution of interfacial dislocations to the effective equation of motion. Upon projecting $\delta\mathcal{F}_{\rm int}/\delta\phi$ and $\delta\mathcal{F}_{\rm coup}/\delta\phi$ onto the interface, we obtain

$$-(\delta v)_n^i=\frac{\epsilon^2}{\gamma}\int dY\frac{d\phi_0}{dY}\Phi'_{\rm sol}\times(\nabla_x b_y-\nabla_y b_x)(\xi-\mathcal{Y}\beta). \tag{C29}$$

We can physically interpret this contribution as follows. First, in the absence of external stresses ($\beta=0$), it is straightforward to show that the above term is positive and hence favors melting of the solid. This is due to the fact that dislocations at the interface give rise to stresses in the vicinity of the interface and the system can reduce its elastic energy by relaxing this energy; a convenient way to eliminate these interfacial dislocations is by melting. In the presence of external stresses, on the other hand, this term vanishes for

$$\xi-\mathcal{Y}\beta\approx\frac{1}{2}\frac{d^2\xi}{dY^2}Y^2-\frac{\mathcal{Y}}{2}\frac{d^2\beta}{dY^2}Y^2=-\frac{1}{2}(\sigma_{tt}^s+\sigma_{tt}^{ns})Y^2=0, \tag{C30}$$

where the derivatives are evaluated at the interface, or

$$\sigma_{tt}^s=-\sigma_{tt}^{ns}. \tag{C31}$$

Therefore, this term does not contribute to the evolution of the interface once the net tangential stress vanishes.

APPENDIX D: MODEL IN THREE SPATIAL DIMENSIONS

As the model stands now, it applies only to two-dimensional systems. In this Appendix we outline an approach to extending the model to three spatial dimensions by employing a model similar to the one introduced in this paper.

First, we note that the dislocation density becomes a second-rank tensor ρ_{ij}, where the first index denotes the direction of the line and the second indicates the direction of the Burgers vector in the following manner: $\int dS_i\rho_{ij}=b_j$ for any surface $\vec{S}$. The conditions that dislocations cannot terminate in the interior of the crystal are $\partial\rho_{ik}/\partial x_i=0$.

However, one can still employ our formulation utilizing the Airy stress function (or the complex auxiliary function)—in this case there is more than one stress function:[37]

$$\nabla^4\chi'_{ij}=-\frac{1}{2}\frac{\partial}{\partial x_k}(\epsilon_{imk}\rho_{jm}+\epsilon_{jmk}\rho_{im}), \tag{D1}$$

and

$$\sigma_{rs}=2\mu\left[\frac{\partial^2\chi'_{rs}}{\partial x_m^2}+\frac{1}{1-\nu}\frac{\partial^2\chi'_{nn}}{\partial x_r\partial x_s}-\frac{1}{1-\nu}\delta_{rs}\frac{\partial^2\chi'_{nn}}{\partial x_m^2}\right]. \tag{D2}$$

In the above, ϵ_{ijk} denotes the antisymmetric unit tensor. It is useful to make the fields massive in the vapor phase if there are free surfaces, as we did in the two-dimensional case

$$\nabla^4\chi'_{ij}+l^{-4}(1-\Phi_{\rm sol})\chi'_{ij}=-\frac{1}{2}\frac{\partial}{\partial x_k}(\epsilon_{imk}\rho_{jm}+\epsilon_{jmk}\rho_{im})$$
$$\equiv\eta_{ij}. \tag{D3}$$

Conservation for the total Burgers vector leads[28] to the following dynamics for ρ_{ij}:

$$\frac{\partial\rho_{ij}}{\partial t}+\epsilon_{ilm}\frac{\partial j_{mj}}{\partial x_l}=0, \tag{D4}$$

where j_{mj} denotes the dislocation flux tensor. It can be shown[38] that the flux tensor can be written as

$$j_{mj}=-B_{mjst}\epsilon_{sab}\frac{\partial}{\partial x_b}\left(\frac{\delta\mathcal{F}}{\delta\rho_{at}}\right), \tag{D5}$$

where a linear relation between thermodynamic forces and fluxes has been assumed; furthermore, for an isotropic system, B_{mjst} becomes

$$B_{mjst}=\tilde{B}[\tfrac{1}{2}(\delta_{mt}\delta_{js}+\delta_{ms}\delta_{jt})-\tfrac{1}{3}\delta_{mj}\delta_{st}], \tag{D6}$$

where $\tilde{B}$ is a constant. When one integrates Eq. (D4) in time, a subtlety is that the auxiliary conditions must be satisfied at all times. However, it is easy to show that if these conditions are satisfied at $t=0$, they are satisfied at all later times. From the equation of motion, Eq. (D4), one obtains

$$\frac{\partial}{\partial t}\frac{\partial\rho_{ij}}{\partial x_i}=-\epsilon_{ilm}\frac{\partial^2 j_{mj}}{\partial x_l\partial x_i}\equiv 0, \tag{D7}$$

since ϵ_{ilm} is antisymmetric in (il) and the partial derivatives are symmetric. Hence, the auxiliary conditions hold at all times.

APPENDIX E: AUXILIARY FIELD ξ IN THE SHARP-INTERFACE LIMIT

In this Appendix we will derive the sharp-interface limit model corresponding to the auxiliary field ξ. This derivation is valid in the limit $l/\Lambda\ll 1$, where Λ denotes the characteristic scale of the film and l is a small parameter related to the correlation length of defects in the liquid phase. For now, we also assume that $\epsilon\ll l$, where ϵ denotes the thickness of the diffuse interface. At the end of the calculation we will comment on this approximation.

Our starting point is Eq. (16),

$$\frac{1}{\mathcal{Y}}\nabla^4\xi+\eta+\frac{1}{\mathcal{Y}l^4}(1-\Phi_{\rm sol})\xi=0, \tag{E1}$$

which can be rearranged to read

$$l^4\nabla^4\xi+(1-\Phi_{\rm sol})\xi=-l^4\mathcal{Y}\eta. \tag{E2}$$

Next we assume that $\phi(\vec{r})\approx\phi_0(Y)$ where $Y=W(x,y)$ denotes the distance to the interface from point (x,y) along a normal to the interface, and $s=S(x,y)$ denotes the arc length along the interface measured from some reference point.

We will solve Eq. (E2) in a perturbation theory in l and show that, to lowest order, l appears through effective boundary conditions applied at the interface. It is essential to note that this is a singular perturbation problem since l multiplies the highest derivative. Therefore, we will solve this problem using the matched asymptotic expansion technique. We proceed by formally expanding ξ in a perturbation series in l, and hence obtain the "outer" expansion: $\xi_0=\Sigma_{n=0}^{\infty}l^n\xi_0^n(\vec{r})$. Substituting this in Eq. (E2) we find that, to lowest order,

$$\nabla^4\xi_0=-\mathcal{Y}\eta_0, \tag{E3}$$

for $Y<0$, and $\xi_0=0$ for $Y>0$, since η vanishes in the liquid phase.

Next we introduce the inner expansion and write $\xi_i=\Sigma_{n=0}^{\infty}l^n\xi_i^n(z)$, where we have introduced the stretched variable $z\equiv Y/l$. Furthermore, to lowest order we can approximately write $(1-\Phi_{\rm sol})\approx\theta(Y)$, where θ denotes the Heaviside step function. Hence, the equation satisfied by the inner expansion becomes

$$l^4\nabla^4\xi+\theta(Y)\xi=-l^4\mathcal{Y}\eta. \tag{E4}$$

Upon substituting this into Eq. (E4) we find that ξ_i^0 satisfies $d^4\xi_i^0/dz^4+\theta(z)\xi_i^0=0$, where we have used the fact that the interface is planar at this level. [Note that Eq. (E4) is effectively one dimensional at this level of approximation—there would be terms at higher order arising from the curvature of the interface. However, these terms turn out to be unimportant at the end of the calculation.] We again note that this approximation is valid for $\epsilon\ll l$; in this case, the order parameter varies very rapidly on the scale of l. Furthermore, since $\xi_0=0$ for $Y>0$, this implies that $\lim_{Y\to\infty}\xi_i^0=\lim_{Y\to\infty}d\xi_i^0/dY=0$. We expect this equation to have an envelope of exponentially decaying solutions for $z>0$. Indeed, it can be verified by a direct substitution that the following solution satisfies the biharmonic equation for $z>0$ and is well behaved for $z\to\infty$:

$$\xi_i^0(z)=\tilde{A}\cos(z/\sqrt{2})\exp(-z/\sqrt{2})$$
$$+\tilde{B}\sin(z/\sqrt{2})\exp(-z/\sqrt{2}). \tag{E5}$$

The constants $\tilde{A}$ and $\tilde{B}$ will be determined by matching the inner and the outer solutions at the origin.

To this end, we first formally solve Eq. (E3) and expand the solution in terms of the stretched variable z in the vicinity of the interface

$$\xi_0=\frac{1}{6}\xi_0'''(0;A,B)l^3z^3+\tfrac{1}{2}\xi_0''(0;A,B)l^2z^2$$
$$+\xi_0'(0;A,B)lz+\xi_0(0;A,B)+\cdots, \tag{E6}$$

where the two integration constants (A,B) parameterize the derivatives of the solution at the interface. In order to determine the unknown constants $(A,B,\tilde{A},\tilde{B})$ we match the inner and outer solutions at the interface $z=0$. Upon requiring that ξ has continuous derivatives up to third order at $z=0$, we obtain the following set of conditions:

$$\tilde{A}=\xi_0(0;A,B),$$

$$-\frac{\tilde{A}}{\sqrt{2}}+\frac{\tilde{B}}{\sqrt{2}}=l\xi_0'(0;A,B),$$

$$\tilde{B}=l^2\xi_0''(0;A,B),$$

$$\frac{\tilde{A}}{\sqrt{2}}+\frac{\tilde{B}}{\sqrt{2}}=l^3\xi_0'''(0;A,B), \tag{E7}$$

where we have employed the explicit solution Eq. (E5). Taking the limit $l\to 0$ trivially yields $\tilde{A}=\tilde{B}=0$ and, therefore,

$$\xi_0(0;A,B)=0, \tag{E8}$$

providing one condition between A and B. Furthermore, upon expanding

$$\tilde{B}=\tilde{B}_0+l\tilde{B}_1+l^2\tilde{B}_2+\cdots \tag{E9}$$

and

$$\xi_0''(0;A,B)=\xi_{o,0}''+l\xi_{o,1}''+l^2\xi_{o,2}''+\cdots \tag{E10}$$

we readily obtain $\tilde{B}_0=\tilde{B}_1=0$, and hence $\tilde{B}=O(l^2)$. Furthermore, from the last condition in Eq. (E7), similar considerations for $\tilde{A}$ yield $\tilde{A}=O(l^2)$. These estimates are valid for $A=O(1)$ and $B=O(1)$.[41] In particular, this implies that $\xi_0(0)=O(l^2)=0$ as $l\to 0$, and $\xi_0'(0)=O(l)=0$, as $l\to 0$, which we recognize as two effective boundary conditions at the interface. In other words, we have just shown that the phase-field equation $l^4\nabla^4\xi+(1-\Phi_{\rm sol})\xi=-l^4\mathcal{Y}\eta$ is equivalent to $\nabla^4\xi=-\mathcal{Y}\eta$ in the domain $\Omega=\{\phi(\vec{r})=1\}$ with $\xi=\boldsymbol{\nabla}\xi\cdot\vec{n}=0$ at the interface $\{\phi(\vec{r})=1/2\}$ in the limit $l\to 0$.

Physically, the above results are not very surprising. The finite mass term forces ξ to vanish exponentially in the liquid phase, leading to the first boundary condition. On the other hand, all derivatives of ξ are also forced to vanish exponentially fast in the liquid phase. Upon requiring that ξ has finite derivatives up to third order at the interface, we arrive at the second boundary condition.

In the numerics we have employed $\epsilon/l=0.5$. Hence, the Heaviside step function is replaced by a function (essentially the equilibrium order-parameter profile) that varies smoothly on the scale of l, so the inner solution is a more complicated function of z, than the one above. Nevertheless, asymptotically it must decay exponentially, since $[1-\Phi_{\rm sol}(z)]\to 1$ as $z\to\infty$. This implies that the asymptotic solution is the one given in Eq. (E5). Therefore, in the limit $l\to 0$ we may use similar arguments to those above, obtaining the same two boundary conditions. As well, a finite $\epsilon\approx l$ will generate additional l-dependent terms in the boundary values of ξ and its first derivative.

*Present address: Department of Mechanical and Aerospace Engineering and Princeton Materials Institute, Princeton University, Princeton, NJ 08544.

[1] R.J. Asaro and W.A. Tiller, Metall. Trans. **3**, 1789 (1972).
[2] M. Grinfeld, Dokl. Akad. Nauk SSSR **290**, 1358 (1986) [Sov. Phys. Dokl. **31**, 831 (1986)].
[3] D.J. Srolovitz, Acta Metall. **37**, 621 (1989).
[4] B.J. Spencer, P.W. Voorhees, and S.H. Davis, Phys. Rev. Lett. **67**, 3696 (1991).
[5] W.H. Yang and D.J. Srolovitz, Phys. Rev. Lett. **71**, 1593 (1993).
[6] J.E. Guyer and P.W. Voorhees, Phys. Rev. Lett. **74**, 4031 (1995).
[7] J. Müller and M. Grant, Phys. Rev. Lett. **82**, 1736 (1999).
[8] K. Kassner and C. Misbah, Europhys. Lett. **46**, 217 (1999).
[9] H. Gao and W.D. Nix, Annu. Rev. Mater. Sci. **29**, 173 (1999).
[10] F.C. Frank and J.H. van der Merwe, Proc. R. Soc. London, Ser. A **198**, 205 (1949).
[11] J.H. van der Merwe, J. Appl. Phys. **34**, 123 (1962).
[12] J.W. Matthews and A.E. Blakeslee, J. Cryst. Growth **27**, 118 (1974).
[13] J.W. Matthews, J. Vac. Sci. Technol. **12**, 126 (1975).
[14] D.E. Jesson, S.J. Pennycook, J.-M. Baribeau, and D.C. Houghton, Phys. Rev. Lett. **71**, 1744 (1993); D.E. Jesson, K.M. Chen, S.J. Pennycook, T. Thundat, and R.J. Warmack, Science **268**, 1161 (1995).
[15] J. Tersoff and F.K. LeGoues, Phys. Rev. Lett. **72**, 3570 (1994).
[16] A.G. Cullis, A.J. Pidduck, and M.T. Emery, Phys. Rev. Lett. **75**, 2368 (1995).
[17] C.S. Ozkan, W.D. Nix, and H. Gao, Appl. Phys. Lett. **70**, 2247 (1997).
[18] E. Granato, J.M. Kosterlitz, and S.C. Ying, Phys. Rev. B **39**, 3185 (1989).
[19] D.J. Eaglesham and M. Cerullo, Phys. Rev. Lett. **64**, 1943 (1990).
[20] P. Nozières, J. Phys. I **3**, 681 (1993).
[21] J. Müller, Ph.D. thesis, McGill University, 1998.
[22] W.H. Yang and D.J. Srolovitz, J. Mech. Phys. Solids **42**, 1551 (1994).
[23] K. Kassner, C. Misbah, J. Müller, J. Kappey, and P. Kohlert, Phys. Rev. E **63**, 036117 (2001).
[24] L. Dong, J. Schnitker, R.W. Smith, and D.J. Srolovitz, J. Appl. Phys. **83**, 217 (1998).
[25] K.W. Schwarz, J. Appl. Phys. **85**, 108 (1999); **85**, 120 (1999).
[26] In the approach of K. R. Elder, M. Katakowski, Mikko Haataja, and Martin Grant (unpublished), one simulates the ''atoms'' themselves with a phase-field approach.
[27] Mikko Haataja, Judith Müller, A.D. Rutenberg, and Martin Grant, Phys. Rev. B **65**, 035401 (2002).
[28] L. Landau and E. M. Lifshitz, *Theory of Elasticity* (Pergamon Press, Oxford, 1986).
[29] K. Aguenaou, Ph.D. thesis, McGill University, 1997.
[30] F. R. N. Nabarro, *Theory of crystal dislocations* (Dover Publications, New York, 1967).
[31] K.R. Elder, Martin Grant, Nikolas Provatas, and J.M. Kosterlitz, Phys. Rev. E **64**, 021604 (2001).
[32] R. Kobayashi, Physica D **63**, 410 (1993).
[33] D.R. Nelson, Phys. Rev. B **18**, 2318 (1978).
[34] D.R. Nelson and B.I. Halperin, Phys. Rev. B **19**, 2457 (1979).
[35] We note that with this convention for the net strain, dislocations with $b_x>0$ at the film-substrate interface will screen a tensile stress in the film, while in practice there will be dislocations with $b_x<0$ at the interface. This difference is due to the fact that, in our formulation, dislocations screen the local stress,

whereas in misfitting films, dislocations form and let the bulk of the film relax to its equilibrium state. This is not significant since we will show below that our formulation is in agreement with the well-known Matthews-Blakeslee (Ref. 12) condition for the appearance of misfit dislocations.

[36] S.Y. Hu and L.Q. Chen, Acta Mater. **49**, 1879 (2001).

[37] Due to the symmetry of χ'_{ij}, there are six components. However, it can be shown that only three components are independent; see Refs. 28, 30, and 38.

[38] J.M. Rickman and J. Viñals, Philos. Mag. A **75**, 1251 (1997).

[39] A. Onuki and H. Nishimori, Phys. Rev. B **43**, 13 649 (1991).

[40] C. Sagui, A.M. Somoza, and R.C. Desai, Phys. Rev. E **50**, 4865 (1994).

[41] We have explicitly verified that the following simpler problem obeys this scaling: $l^4 d^4\xi/dz^4 + \theta(z-u)\xi = 0$ for $0 \leqslant z \leqslant 1$ with $\xi(0) = \xi'(0) = 1$ and $\xi(1) = \xi'(1) = 0$.